HHS Public Access

Author manuscript

Neuron. Author manuscript; available in PMC 2018 November 13.

Published in final edited form as:

Neuron. 2017 October 11; 96(2): 387–401.e6. doi:10.1016/j.neuron.2017.09.044.

Loss of CLOCK Results in Dysfunction of Brain Circuits Underlying Focal Epilepsy

Peijun Li[1,15,*], **Xiaoqin Fu**[1,2,15], **Nathan A. Smith**[1], **Julie Ziobro**[1], **Julian Curiel**[1], **Milagros J. Tenga**[3], **Brandon Martin**[1], **Samuel Freedman**[4], **Christian A. Cea-Del Rio**[4], **Livio Oboti**[1], **Tammy N. Tsuchida**[5], **Chima Oluigbo**[5,6], **Amanda Yaun**[5,6], **Suresh N. Magge**[5,6], **Brent O'Neill**[7], **Amy Kao**[5], **Tesfaye G. Zelleke**[5], **Dewi T. Depositario-Cabacar**[5], **Svetlana Ghimbovschi**[8], **Susan Knoblach**[8], **Chen-Ying Ho**[8,9,13], **Joshua G. Corbin**[1], **Howard P. Goodkin**[10], **Stefano Vicini**[11], **Molly M. Huntsman**[4], **William D. Gaillard**[1,5], **Gregorio Valdez**[3,12], and **Judy S. Liu**[1,14,16,*]

[1]Center for Neuroscience Research, Children's Research Institute, Children's National Medical Center, Washington, DC 20010, USA

[2]The Second Affiliated Hospital and Yuying Children's Hospital of Wenzhou Medical University, Wenzhou, Zhejiang 325027, China

[3]Virginia Tech Carillion Research Institute; Roanoke, VA 24014, USA

[4]Department of Pharmaceutical Sciences, Skaggs School of Pharmacy and Pharmaceutical Sciences, Department of Pediatrics, School of Medicine, University of Colorado Anschutz Medical Campus, Aurora, CO 80045, USA

[5]Comprehensive Pediatric Epilepsy Program, Division of Neurophysiology and Epilepsy, Children's National Health Medical Center; Washington, DC 20010 USA

[6]Division of Neurosurgery, Children's National Medical Center, Washington, DC 20010, USA

[7]Division of Pediatric Neurosurgery, School of Medicine, University of Colorado, Anschutz Medical Campus, Aurora, CO 80045, USA

[8]Center for Genetic Medicine, Children's Research Institute, Children's National Medical Center, Washington, DC 20010, USA

[*]Correspondence: peijun.li@va.gov (P.L.), judy_liu@brown.edu (J.S.L.).

AUTHOR CONTRIBUTIONS

J.S.L., P.L., and X.F. conceived and designed this study; coordinated the collaborations with clinical services and the laboratories of G.V., M.M.H., H.P.G., and S.V.; assisted with data analysis and interpretation; and wrote the manuscript. The clinical neurophysiology team for evaluation of patients and intraoperative EEG consisted of W.D.G., T.N.T., A.K., T.G.Z., D.T.D.-C., and H.P.G. A.Y., C.O., S.N.M., and B.O. are neurosurgeons, and they performed the resections on patients enrolled in this study and collaborated with laboratory members J.C. and S.F. for collection of tissue. C.-Y.H. performed the diagnostic neuropathology on human tissue included in this study. Wholecell patch-clamp electrophysiology on human tissue was performed by P.L., B.M., C.A.C.-D.R., S.F., and L.O. with their respective principal investigators: J.S.L., M.M.H., and J.G.C. S.G. and S.K. performed the microarray and gene expression analysis. G.V. and M.J.T. generated the mice with conditional *Clock* deletions in excitatory and inhibitory neurons. X.F. performed western analysis and immunostaining of human and mouse tissue. X.F. and M.J.T. performed image analysis. J.C. graded seizure behavior in mice. N.A.S. and J.Z. performed the mouse EEG with guidance from H.P.G. P.L. designed and performed the whole-cell patch-clamp electrophysiology experiments on mice with guidance from J.S.L. and S.V.

SUPPLEMENTAL INFORMATION

Supplemental Information includes seven figures, four tables, and two movies and can be found with this article online at https://doi.org/10.1016/j.neuron.2017.09.044.

[9]Division of Pathology, Children's National Medical Center; Washington, DC 20010, USA

[10]Departments of Neurology and Pediatrics, University of Virginia Health System, Charlottesville, VA 22908, USA

[11]Department of Pharmacology and Physiology, Georgetown University, Washington, DC 20057, USA

[12]Department of Biological Sciences, Virginia Tech; Blacksburg, VA 24061, USA

[13]Present address: Department of Pathology, University of Maryland School of Medicine, Baltimore, MD 21201, USA

[14]Present address: Department of Neurology, Department of Molecular Biology, Cell Biology, and Biochemistry, Brown University, Providence, RI 02903, USA

[15]These authors contributed equally

[16]Lead Contact

SUMMARY

Because molecular mechanisms underlying refractory focal epilepsy are poorly defined, we performed transcriptome analysis on human epileptogenic tissue. Compared with controls, expression of *Circadian Locomotor Output Cycles Kaput* (*CLOCK*) is decreased in epileptogenic tissue. To define the function of CLOCK, we generated and tested the *Emx-Cre; Clock*$^{flox/flox}$ and *PV-Cre; Clock*$^{flox/flox}$ mouse lines with targeted deletions of the *Clock* gene in excitatory and parvalbumin (PV)-expressing inhibitory neurons, respectively. The *Emx-Cre; Clock*$^{flox/flox}$ mouse line alone has decreased seizure thresholds, but no laminar or dendritic defects in the cortex. However, excitatory neurons from the *Emx-Cre; Clock*$^{flox/flox}$ mouse have spontaneous epileptiform discharges. Both neurons from *Emx-Cre; Clock*$^{flox/flox}$ mouse and human epileptogenic tissue exhibit decreased spontaneous inhibitory post-synaptic currents. Finally, video-EEG of *Emx-Cre; Clock*$^{flox/flox}$ mice reveals epileptiform discharges during sleep and also seizures arising from sleep. Altogether, these data show that disruption of CLOCK alters cortical circuits and may lead to generation of focal epilepsy.

In Brief

Li, Fu, et al. find that expression of the circadian transcription factor CLOCK is decreased in the "seizure focus" from patients with intractable epilepsy and that CLOCK loss of function in cortical excitatory neurons is sufficient for epileptogenesis in mouse.

INTRODUCTION

Epilepsy, a disorder of recurrent unprovoked seizures, is a common disabling neurological condition affecting up to 1 in 26 individuals (England et al., 2012; Hauser et al., 1993; Hesdorffer et al., 2011). While single gene mutations in ion channels or neurotransmitter receptors are associated with generalized, inherited forms of epilepsy (Helbig et al., 2008; Lerche et al., 2013; Mantegazza et al., 2010), genetic causes do not account for the majority of patients with the disorder. Most patients have focal epilepsy, and their seizures arise from

discrete pathological regions of abnormal brain tissue. Surgical resection of the “focus,” where seizures originate, often ameliorates refractory, medication-resistant epilepsy (Englot and Chang, 2014). Despite its clinical importance, the molecular mechanisms defining epileptogenic tissue are poorly understood.

To determine molecular signatures of focal epilepsies, we have collected brain samples obtained from therapeutic resections of epileptogenic tissue associated with two common causes of focal epilepsy: focal cortical dysplasia (FCD) and tuberous sclerosis complex (TSC). FCD is the most common cause of intractable focal epilepsy in the U.S. pediatric population, and about 45% of all epilepsy surgery is performed for FCD (Lerner et al., 2009). FCD is a heterogeneous disorder (Blümcke et al., 2011), but some subtypes demonstrate abnormal activation of the mammalian target of rapamycin (mTOR) pathway. The basis of this change may be somatic mutations in genes upstream of mTOR, including PI3-Kinase catalytic subunit alpha (PIK3CA) (Jansen et al., 2015) or germline mutations in disheveled, Egl-10, and pleckstrin domain-containing protein 5 (DEPDC5) (D’Gama et al., 2015; Scheffer et al., 2014). In many cases, even though no specific mutation has been found, abnormal mTOR function is observed (Jansen et al., 2015; Wong, 2013). In contrast, the neurodevelopmental disorder TSC is caused by heritable heterozygous mutations in either the TSC1 or the TSC2 (TUBERIN) genes, which encode repressors of the mTOR pathway (Narayanan, 2003). Despite the fact that upregulation of mTOR activity occurs throughout the entire brain, patients with TSC have focal seizures arising from discrete regions with disruption of cortical architecture (reviewed in Crino et al., 2006). While mTOR is undoubtedly important for regulating many aspects of neuronal function, this disparity, as well as incomplete suppression of seizures by mTOR inhibitors (Zeng et al., 2008), indicates that additional molecular analysis is needed to understand the initiation and progression of epilepsy.

Here, we show a decrease in Circadian Locomotor Output Cycles Kaput (CLOCK) expression in epileptogenic tissues associated with FCD and TSC. CLOCK is a transcription factor whose function in the suprachiasmatic nucleus regulates circadian rhythm. However, it is expressed in nearly all tissues (Antoch et al., 1997; King et al., 1997). In the cerebral cortex, its role is not fully understood. Nevertheless, the binding partner of CLOCK, the brain muscle ARNT-like 1 (BMAL1), alters seizure threshold in mice (Gerstner et al., 2014) and also regulates the mTOR pathway (Lipton et al., 2015). Furthermore, epilepsy has a known association with the sleep/wake cycle (Bourgeois, 1996). Our data show that principal neurons deficient in CLOCK have defects in spontaneous inhibitory postsynaptic currents, resulting in increased excitability. Furthermore, *Emx-Cre; Clock*$^{flox/flox}$ mice with conditional deletion of Clock in excitatory neurons exhibit seizures associated with sleep, a common feature of human focal epilepsy. We conclude that defects in CLOCK-mediated gene expression may lead to changes in cortical circuits underlying human focal epilepsy.

RESULTS

CLOCK Is Reduced in Human Epileptogenic Tissue

We sought to identify molecular signatures associated with epileptogenic tissue. Thus, we collected surgical specimens from therapeutic resections for treatment of focal epilepsy

under the supervision of our respective institutional review boards. In our initial experiments, after obtaining consent and assent when appropriate, we collected tissues from patients with two common etiologies of focal epilepsy: FCD and TSC (Table S1). In these patients, the location and extent of the epileptogenic focus was defined using high-resolution 3T MRI (Figures 1A and 1B) and intraoperative electrocorticography (ECoG) (Figures 1C–1E) (Chang et al., 2011). Samples were collected directly from the operating room within 5 min of removal of the tissue from the blood supply and put into chilled, oxygenated artificial cerebral spinal fluid (ACSF). After clearance from pathology, samples were processed for research.

In addition to the epileptogenic focus, we sought to obtain control tissue. Autopsy tissue from patients without seizures is not handled in the same way as surgical tissue and thus not an appropriate control. However, we obtained a limited number of surgical samples without epileptiform activity that also appeared radiologically normal. This control tissue would not ordinarily be removed except that removal was necessary to reach underlying regions of epileptogenic tissue. Although the tissue is from patients with epilepsy and may be activated when patients have seizures, it is the best available control and is matched with seizure tissue for age, medication profile, and genetic background.

Using microarray analysis, we compare transcriptomes of five cases of epileptogenic tissue from FCD cases to those of three control samples. We also compare epileptogenic regions from three TSC cases to the same control samples. Two of the epileptogenic FCD samples are matched with adjacent control tissue from the same patient. Two of the TSC cases have confirmed causative mutations in TSC2, and genetic testing was not performed on the other case (Table S1). A one-way ANOVA statistical test ($p < 0.05$) was applied in Partek to compare normalized mRNA expression levels between control tissue, epileptogenic tissue from FCD, and epileptogenic tissue from TSC.

Transcriptome analysis shows commonalities between FCD and TSC cases demonstrating large-scale transcriptome changes compared with the control (Figure 2A), and graphs of the distribution of p values demonstrate significant differences between groups (Figure S1). However, after application of the step-up false discovery rate multiple test adjustment (Benjamini and Hochberg, 1995) and a 1.5-fold cutoff, only 23 downregulated genes and 26 upregulated genes remain that are changed for both FCD and TSC (Table S2). Among these changes, the decreases in *CLOCK* mRNA expression are notable because of their p values in both FCD and TSC cases. In both FCD and TSC groups, when changes in expression are sorted by p value, changes in *CLOCK* expression have the smallest p values of those downregulated genes with known functions (0.00086 and 0.00055 for FCD and TSC, respectively).

Because microarray data can be technically inconsistent and requires validation (Morey et al., 2006), we performed western blot analysis to confirm our findings and establish whether changes in CLOCK protein levels are consistent with reduction in the mRNA. We included other etiologies of focal epilepsy (Table S1). Results by western blot analysis indicate that CLOCK levels are significantly reduced (Figures 2C, with uncropped western blot results in Figure S2A). We analyzed different subtypes of FCD, but also included TSC, and one case

of Rasmussen's encephalitis. CLOCK protein levels are reduced by more than 30% or more in 12 cases out of a total of 18 cases (Table S1). CLOCK was reduced by 25% in the one case of Sturge-Weber that we tested (Table S1). No significant change is found in our hemimegalencephy case (Table S1). In the FCD cases with decreased CLOCK, we examined other components of the main circadian regulatory loop. BMAL1 gene, which dimerizes with CLOCK and regulates seizure threshold in mice (Gerstner et al., 2014), is unchanged in epileptogenic FCD tissues (Figure 2C). In contrast, we find that Cryptochrome (Cry) and Period (Per) proteins, downstream targets of CLOCK/BMAL1, are significantly decreased (Figure 2C; Figure S2A). Normally, the CLOCK/BMAL1 transcription complex binds to promoter regions of *Cry* and *Per* to stimulate their gene expression. In turn, Cry and Per are the negative feedback regulators of *Clock* transcription complex. Without customary CLOCK/BMAL activity, expression of downstream targets appears to be altered. Consistent with changes in downstream targets, there is a marked reduction in albumin D-site-binding protein (DBP) in epileptogenic tissue (Figure 2C; Figure S2A). DBP is among known CLOCK targets in the brain, which have been implicated in epilepsy (Gachon et al., 2004). In contrast, we did not find changes in levels of general neuronal markers (Figure 2D).

CLOCK Levels Are Significantly Decreased in Neurons from Epileptogenic Tissue

To determine how CLOCK protein expression changes in epileptogenic tissue, we first analyzed its normal expression pattern in human cortex. CLOCK co-localizes with NeuN-expressing neurons (Figure 2E; Figure S2B). 84% (±2.4%) NeuN cells are CLOCK positive, while 63% (±3.9%) of CLOCK cells are NeuN positive. CLOCK co-localizes with Brain-2 (Brn2), a marker for excitatory neurons in layers 2, 3, and 5 (Figure 2F; Figure S2C). 46% (±2.9%) of Brn2 cells are CLOCK positive, while 80% (±3.5%) of CLOCK cells are Brn2 positive. In the epileptogenic focus (EF), CLOCK is reduced in both NeuN- and Brn2-expressing neurons (Figures 2E and 2F), most of which are excitatory neurons (Chattopadhyaya et al., 2004). Furthermore, in the control tissue from human brain, CLOCK is expressed in parvalbumin (PV)-expressing inhibitory neurons, also known as "fast-spiking" interneurons (Figure 2G). 53%(±4.6%) of PV-positive cells are CLOCK positive, while 10%(±1%) of CLOCK cells are PV positive. In the epileptogenic focus, PV-positive neurons have an average decrease of CLOCK expression by 21%($p = 0.04$). In contrast, the average decrease of CLOCK in Brn2-positive neurons from epileptogenic focus is 44% and comparatively more significant ($p < 0.001$; Figures 2F and 2G).

Similar to its expression in human tissue, CLOCK protein colocalizes with excitatory layer markers Brn2 in mouse cortex (Figure S2D). Overall, 52% (±3%) of Brn2 cells are CLOCK positive, while 86% (±4%) of CLOCK cells are Brn2 positive. In addition, in lateral and caudal regions of the cortex, CLOCK is expressed predominantly in layer 5, as determined by co-localization with CTIP-2 (Figure S2E), in contrast to human cortex, where expression is consistently widespread throughout the layers (Figures S2B and S2C). In mouse cortex, 66% (±4%) of PV-expressing interneurons express CLOCK, and 22% (±5%) of Calbindin-expressing interneurons express CLOCK (Figures S2F and S2G), similar to previous studies (Kobayashi et al., 2015). CLOCK is not detectable in cells expressing markers for astrocytes (GFAP) and oligodendrocytes (CNP) (Figure S2H). Since our human samples are from pediatric cases, we examined CLOCK expression in developing mouse cortex by western

blot analysis. CLOCK levels are high in embryonic stages, with consistent expression past weaning age (Figure S2I). Furthermore, consistent with previous studies, CLOCK protein expression in cortex does not vary according to the 24-hr day/night cycle (data not shown) (Kobayashi et al., 2015).

Emx-Cre; Clock$^{flox/flox}$ Mice Have Diminished Seizure Threshold

Because CLOCK expression is reduced in both excitatory and PV-expressing inhibitory neurons in human epileptogenic tissue, we sought to use conditional mouse genetic models to determine the function of the CLOCK transcription factor in epileptogenic brain tissue. In the *PV-Cre; Clock*$^{flox/flox}$ mouse (Debruyne et al., 2006; Hippenmeyer et al., 2005), the *Clock* gene is deleted in PV-expressing interneurons in the cortex (Figure 3A). This deletion of *Clock* in PV interneurons has no significant effect on seizure threshold as determined by the behavioral response to pentylenetetrazol (PTZ) (Figure 3B). Because of the variability in appearance of behavioral seizures, we also use video EEG for a more sensitive measure of seizure onset (Figures 3C–3F). The appearance of epileptiform discharges and seizures are not significantly different between control *PV-Cre* and *PV-Cre; Clock*$^{flox/flox}$ animals. Furthermore, the averaged power spectra of EEGs are unchanged, as well (Figure 3F).

In contrast, in the *Emx-Cre; Clock*$^{flox/flox}$ mouse cortex, the *Clock* gene is deleted in excitatory neurons (Gorski et al., 2002), which comprise 70% of neurons in the cortex, but is intact in PV-expressing interneurons (Figure 3G). In contrast to *PV-Cre; Clock*$^{flox/flox}$ animals, seizure threshold is decreased in *Emx-Cre; Clock*$^{flox/flox}$ mice. The latency to generalized tonic-clonic seizures (GTC) is significantly reduced in *Emx-Cre; Clock*$^{flox/flox}$ mice with conditional deletion of the *Clock* gene in excitatory neurons following administration of PTZ (Figure 3H). Since we do not observe a significant change in the onset of milder seizures in *Emx-Cre Clock*$^{flox/flox}$ mice, we use video EEG to increase the sensitivity of seizure detection. With video-EEG recording, we are also able to detect an earlier onset of seizures in the *Emx-Cre; Clock*$^{flox/flox}$ than in the control *Emx-Cre* mouse in response to PTZ (Figures 3I–3K). Furthermore, analysis of the first 15 minutes of EEG recording after PTZ administration demonstrates change in the power spectrum of the EEG (Figure 3L) with an increase in amplitude of the voltage in the lower frequencies, consistent with a greater response to PTZ. Thus, CLOCK loss of function in excitatory neurons results in greater cortical excitability in mice and may play an important role for epileptogenesis in human focal epilepsy. This result is not due to a primary change in the regulation of the sleep/wake cycle via the suprachiasmatic nucleus (SCN), since CLOCK is preserved in the SCN of the *Emx-Cre; Clock*$^{flox/flox}$ mouse (Figure S3). Rather, the decreased seizure threshold is a direct effect of selective deletion of *Clock* in the cortical excitatory neurons.

PAR bZip Transcription Factors, Downstream Targets of CLOCK, Are Reduced in Human Epileptogenic Tissue and Emx-Cre; Clock$^{flox/flox}$ Mouse Cortical Lysates

Among known direct CLOCK targets in the brain, the proline- and acidic amino acid-rich basic leucine zipper (PAR bZip) transcription factors have been implicated in epilepsy (Gachon et al., 2004). We therefore assayed expression of these transcription factors in human epilepsy tissue and *Emx-Cre; Clock*$^{flox/flox}$ mouse cortex. As noted above, there is a marked reduction in DBP in epileptogenic tissue (Figure 2C). We then asked whether this

reduction was also observed in the *Emx-Cre; Clock*$^{flox/flox}$ mice. Of the three PAR bZip transcription factors, DBP and the hepatic leukemia factor (HLF) are significantly lower in *Emx-Cre; Clock*$^{flox/flox}$ cortex as compared to control (Figure S4A). These findings demonstrate disruption of CLOCK-mediated transcriptional activity in both human and our mouse model.

Neurons from Epileptogenic Tissue and Emx-Cre; Clock$^{flox/flox}$ Mice Have Spine Defects

To understand how CLOCK loss of function relates to human focal epilepsy with decreased CLOCK expression, we compared the *Emx-Cre; Clock*$^{flox/flox}$ mice to human FCD. Disruption of the layered structure or lamination of cortical neurons is common in both FCD (Fauser et al., 2013; Thom et al., 2005) and TSC (Muhlebner et al., 2016). Because CLOCK is expressed in embryonic stages when neurons are migrating (Figure S2I), and the conditional deletion of the *Clock* gene also occurs during embryonic stages, we first determined whether the position of cortical neurons is normal in *Emx-Cre; Clock*$^{flox/flox}$ mice. We find that both upper cortical layers and lower cortical layers are normal in terms of neuronal identity and position based on distribution of Cux1 positive neurons (Figure 4A), CTIP-2 neurons (Figure 4A), and Brn2 neurons (data not shown). Although we were not able to immunostain for specific neuronal layers in human tissue, the epileptogenic tissue from FCD cases in our study have abnormal neuronal density and distribution consistent with known defects (Fauser et al., 2013; Thom et al., 2005) (Figure 4B). Thus, *Emx-Cre; Clock*$^{flox/flox}$ mice do not phenocopy the laminar defects seen in FCD cases.

We next examined dendritic structure, since some subtypes of FCD and TSC cases have abnormally large neurons with altered dendrites (Blümcke et al., 2011; Tavazoie et al., 2005). We find that Sholl analysis of biocytin-filled neurons in the *Emx-Cre; Clock*$^{flox/flox}$ mice demonstrates the same distribution of dendrites as that of the *Emx-Cre* control mice (Figure S4B). In contrast, Sholl analysis of human biocytin-filled neurons from FCD cases shows abnormally high numbers of dendritic crossings closer to the cell body and a decrease in dendritic crossing distally (Figure S4C). Thus, early stages in neuronal development appear to be normal in the *Emx-Cre; Clock*$^{flox/flox}$ mice, and the changes in seizure threshold in *Emx-Cre; Clock*$^{flox/flox}$ mice are not due to defects in neuronal migration and dendritogenesis.

Although lamination and dendritic branching is normal in *Emx-Cre; Clock*$^{flox/flox}$ neurons, these *Clock*-deficient neurons have defects in dendritic spines, which are similar to spine defects observed in tissue from human epileptogenic FCD cases (Figures 4C–4H). Morphological studies of biocytin-filled layer 5 pyramidal neurons from *Emx-Cre* and *Emx-Cre; Clock*$^{flox/flox}$ mice reveal a region-specific decrease in spines, with a decrease in spine density in the apical dendrite and primary branches, but not in secondary and tertiary branches or in basal dendrites of *Clock*-deficient neurons (Figures 4C–4E). To determine whether acute reduction of CLOCK protein also results in spine defects, we used short hairpin RNA interference (shRNAi) to target *Clock* mRNA in dissociated cultures (Figures S4D–S4H; Table S3). Within 72 hr of transfection with the construct, pyramidal neurons exhibit fewer spines. Those remaining have predominately immature spine morphologies (Figures S4E–S4H). These phenotypes occur using two constructs targeting different regions

of the *Clock* mRNA. While a CLOCK expression construct is able to return spines to mature morphologies (Figure S4G), re-expression of CLOCK transcription factor was not able to rescue spine density (Figure S4H). This may indicate that spine maintenance/formation is dependent on precise regulation of CLOCK activity, either in terms of timing or expression levels.

Because we observed spine defects in mouse, we also examined dendritic spines in human tissue associated with seizures. These morphological alterations are also present in pyramidal neurons within epileptogenic tissue from human patients that have diminished CLOCK protein expression (Figures 4F–4H). Compared with neurons from normal control tissue (4 cases, n = 21 neurons), neurons from epileptogenic foci (5 cases, n = 23 neurons) had reduced spine density in just apical and primary dendrite, but not the basal dendrite (Figures 4F–4H; Table S1), which is similar to the neurons from *Emx-Cre; Clock*$^{flox/flox}$ mice. Thus, the spine defect in epileptogenic tissue correlates strongly with the mouse model with the *Clock* gene deleted in excitatory neurons.

L5 Pyramidal Neurons in Emx-Cre; Clock$^{flox/flox}$ Mice Have Increased Excitability

To determine the functional relevance of CLOCK at a cellular level, we performed whole-cell recordings in L5 somatosensory cortical pyramidal neurons, where CLOCK is predominantly expressed (Figure S2D). From the spontaneous excitatory postsynaptic currents (sEPSC) and miniature excitatory postsynaptic currents (mEPSCs) recorded in *Emx-Cre; Clock*$^{flox/flox}$ and control neurons, we find a decreased amplitude in sEPSCs (Figure 5A) and a small, but statistically significant, decrease in the frequency of mEPSCs (Figure 5B), which is consistent with the spine defect described above (Figures 4C–4E). Despite the reduction in spontaneous and mEPSCs, we observe frequent polyspike events, also known as paroxysmal depolarizing shifts (PDSs), in *Emx-Cre; Clock*$^{flox/flox}$ mice during measurement of excitatory currents (Figures 5C and 5D). PDS events are cellular correlates of epileptiform discharges. Thus, the net effect of CLOCK loss of function on L5 neurons might be an increase in excitability of the circuit containing the L5 principal neuron.

If CLOCK loss-of-function results in increased excitability, it should result in increased action potential firing, as well. Using cell-attached recordings, we show that L5 pyramidal neurons deficient in CLOCK fired action potentials sooner than that of control neurons when $[K^+]$ in the ACSF is raised to 10 mM through bath application to increase neuronal excitability (Figures S5A and S5B). Furthermore, the depolarizing extracellular K^+ concentration results in higher frequency of action potentials, after onset of action potential firing (Figures S5C and S5D). Analysis of time after raising extracellular $[K^+]$ versus the number of action potentials fired demonstrates an increase in firing rate of action potentials in *Clock*-deficient neurons as compared with controls (Figures S5C and S5D). In order to show the consistency of our wash in time of 10 mM K^+, we used the same setup and performed bath application of extrasynaptic $GABA_A$ receptor δ subunit antagonist THIP (20 μM) in a separate experiment as a control (Figure S5E). We find that the tonic current begins 45.3 (±4.97) s after starting the THIP application (Krook-Magnuson et al., 2008). The variability (about 11.7 s) is much smaller than the latency of firing in both control and *Clock*-deficient neurons, which is around 200 s and 180 s, respectively. Furthermore, the

effect of THIP application occurs much sooner than the onset time of action potentials in 10 mM K^+ bath application. Thus, we can demonstrate the variability of wash-in is unlikely to account for differences in stimulated action potential firing. The change we observe in action potential firing indicates that the end result of disruption of CLOCK-mediated transcriptional activity is an increase in excitability in cortical microcircuits involving L5 neurons. These results correlate with decreased seizure threshold in *Emx-Cre; Clock*$^{flox/flox}$ mice.

L5 Pyramidal Neurons in Emx-Cre; Clock$^{flox/flox}$ Mice Have Defects in Their Spontaneous Inhibitory Postsynaptic Currents

Since L5 pyramidal neurons in *Emx-Cre; Clock*$^{flox/flox}$ mice have frequent PDS events and have increased action potential firing despite decreased amplitude of sEPSCs, we examined whether reduced inhibitory input to these neurons might be the basis of increased circuit excitability. We find that spontaneous inhibitory postsynaptic currents (sIPSCs) have significantly reduced amplitude and frequency but increased rise time and decay time in *Clock*-deficient neurons from *Emx-Cre; Clock*$^{flox/flox}$ mice compared to control mice (Figure 6A). In particular, the decrease in frequency is highly significant ($p = 0.00032$). To determine whether the decrease in inhibition is also a feature of human focal epilepsy, we also performed whole-cell electrophysiology on FCD cases. Intrinsic properties of deeper layer excitatory neurons are not significantly different between control and epileptogenic tissue (Table S4). We examined sIPSCs in pyramidal neurons from a number of cases (four separate controls and five FCD). We find a significant decrease in sIPSC frequency in human epileptogenic FCD tissue and a small, but significant, change in rise time, while amplitude and decay constant are not significantly altered (Figure 6B). Thus, alterations in inhibition of pyramidal neurons in human epileptogenic tissue are similar to those found in the *Emx-Cre; Clock*$^{flox/flox}$ mouse despite considerable heterogeneity in genetics, gender, age, and anti-convulsant usage in patients.

We sought to identify the basis of the change in inhibition. Because it is known that there is a loss in interneurons in human FCD cases, we counted PV-expressing, fast-spiking interneuron density in cortex of *Emx-Cre; Clock*$^{flox/flox}$ mice. We did not find a loss in the number or change in position of PV-expressing, fast-spiking interneurons or PV protein levels in mouse cortex (Figures S6A and S6B). Because these were unchanged, we examined PV-expressing interneurons. For the PV interneurons, intrinsic properties are no different (data not shown). In addition, sEPSCs in PV interneurons, which are also unchanged for the *Emx-Cre; Clock*$^{flox/flox}$ as compared with control *Emx-Cre* mice (Figure S6C). While this doesn't rule out defects in other interneuron sub-populations, neither numbers nor excitability for PV cells were altered in *Emx-Cre; Clock*$^{flox/flox}$ mice.

Because cell numbers and excitability are unchanged in PV interneurons, we next sought to determine whether synapses are altered in the *Emx-Cre; Clock*$^{flox/flox}$ mouse. We performed immunostaining for inhibitory synaptic proteins. Expression levels of both the presynaptic vesicular GABA transporter (Vgat) and the postsynaptic protein Gephyrin (Micheva et al., 2010) are decreased (Figures S6D and S6E). We then examined the inhibitory marker synaptotagmin-2 (Syt2), which labels over 97% of all synapses from PV-positive, fast-

spiking interneurons onto the soma of excitatory neurons (Sommeijer and Levelt, 2012). By immunostaining, Syt2 terminals on cell bodies marked by NeuN of *Emx-Cre; Clock*$^{flox/flox}$ mouse are decreased compared to controls (Figure S6F). By western analysis, we demonstrate a statistically significant decrease in Syt2 (Figure S6G), as well. This selective decrease in inhibitory synaptic proteins is a phenotype commonly seen in animal models of epilepsy (Jin et al., 2011). However, we are not able to demonstrate a functional abnormality in inhibitory synapses by electrophysiology. When we record miniature IPSCs (mIPSCs), we find that they were unchanged between *Emx-Cre; Clock*$^{flox/flox}$ and control neurons (Figure S6J) despite the marked changes in levels of inhibitory synaptic proteins. We repeated the study in a cesium-based solution, which can detect synaptic activity further from the cell body, but this again did not demonstrate a difference. Thus, we are unable to functionally demonstrate a change in inhibitory synaptic function. However, this does not preclude other mechanisms that may lead to altered inhibition on these neurons.

Emx-Cre; Clock$^{flox/flox}$ Mice Have Sleep-Related Spontaneous Seizures

However, we clearly show increased excitability through spontaneous epileptiform activity as well as decreased inhibition of the L5 pyramidal neurons from *Emx-Cre; Clock*$^{flox/flox}$ mice. Therefore, we assessed *Emx-Cre; Clock*$^{flox/flox}$ mice for the presence of spontaneous seizures and find an association of seizures in these mice with sleep (Figure 7). We examined the baseline video EEG in both the *Emx-Cre* and *Emx-Cre; Clock*$^{flox/flox}$ mice. The control *Emx-Cre* mice have no observable seizures, even for extended recording periods >24 hr. Furthermore, EEG recordings during sleep and sleep/wake transitions are normal (Figure 7A). In contrast, we find that the *Emx-Cre; Clock*$^{flox/flox}$ mice have frequent interictal epileptiform discharges, including discharges that occur during sleep (Figure 7B; Movie S1). Significantly, the *Emx-Cre; Clock*$^{flox/flox}$ mice also have generalized tonic-clonic seizures arising from sleep (Racine grade 5; Figures 7C–7F; Movie S2). This seizure arises from sleep (Figures 7D and 7E), starting with a generalized spike-wave complex and fast paroxysmal activity (arrow, Figure 7E). The seizure is followed by a period of postictal depression (Figure 7F, arrow). Finally, quantification of the relationship between seizures and sleep demonstrate that a statistically significant proportion of these seizures occurs proximally to cessation of slow-wave sleep (SWS) with around 60% of events starting within 10 s after cessation of SWS (Figure 7G).

As further proof that these events are epileptic, treating these mice with the anticonvulsant phenobarbital (PB) reduces their frequency significantly (Figure 7H). Analysis of baseline EEG in both *Emx-Cre* and *Emx-Cre; Clock*$^{flox/flox}$ mice by comparing averaged power spectra demonstrates increased EEG amplitude in lower frequencies, consistent with frequent epileptiform discharges and cortical excitability in *Emx-Cre; Clock*$^{flox/flox}$ mice (Figure 7I). In contrast, no spontaneous seizures are observed in *PV-Cre; Clock*$^{flox/flox}$ mice even after extended recordings using EEG (Figure S7). Their sleep/wake transitions are normal, and the baseline power spectra are not significantly different from control *PV-Cre* animals (Figure S7C). Thus, loss of *Clock* expression in excitatory neurons causes seizures that arise from sleep. This finding is significant because human epilepsy is characterized by strong associations with sleep and sleep transitions with up to 25% of patients with epilepsy having seizures exclusively in sleep (Carreño and Fernández, 2016). However, the molecular

basis for seizure association with sleep has not been previously defined. CLOCK-mediated gene expression may explain this phenomenon through its effects on regulation of seizure threshold and epileptogenesis.

DISCUSSION

Here, we find that the circadian transcription factor CLOCK is decreased in brain tissue from patients with intractable epilepsy. We show that the *Emx-Cre; Clock*$^{flox/flox}$ mouse with loss of CLOCK in excitatory neurons has decreased seizure thresholds and increased epileptiform discharges during sleep and seizures associated with sleep. Both excitatory neurons from human surgical resections and from the *Emx-Cre; Clock*$^{flox/flox}$ mouse have decreased sIPSCs, increasing excitability of principal neurons. These changes in cortical circuits may underlie epilepsy in both our mouse model and human epilepsy.

How does loss of CLOCK transcriptional activity in excitatory neurons result in the functional defects leading to epilepsy? Microcircuit rearrangements are a known phenomenon in epilepsy (Paz and Huguenard, 2015), and the alteration in CLOCK may be a molecular signature of this process. At the circuit level, the loss of CLOCK results in increased excitability of pyramidal neurons, in spite of absence of changes in intrinsic properties or membrane potential and modest decreases in both spontaneous and miniature EPSCs. In contrast, we observe a marked decreased amplitude and frequency of sIPSCs, suggesting that the increased excitability in the circuit is due to loss of inhibition on principal neurons. Because we see no change in mIPSCs, the decrease in inhibition is not due to loss of synapses or dysfunction of inhibitory synapses at the cell body of the L5 pyramidal neuron. However, inhibitory synaptic defects in distal dendrites are more difficult to detect, and disconnection of these synapses might explain decreased inhibition. Alternatively, decreased frequency in sIPSCs may result from defects in the activity of presynaptic inhibitory neurons. How loss of CLOCK-mediated transcription in excitatory neurons results in impaired inhibitory activity in their presynaptic partners is unknown, but excitatory neurons can modulate the activity of their inhibitory partners (Kuhlman et al., 2013; Trettel and Levine, 2003). Our future studies will determine whether either or both synaptic or circuit changes are a primary result of CLOCK loss of function.

At the molecular level, CLOCK may regulate important pathways for maintaining neuronal homeostasis. Specifically, deletion of *Clock* in neurons has recently been shown to alter three main clusters of gene expression: (1) synaptic function, (2) mitochondrial function, and (3) ATPase activity (Kobayashi et al., 2015). While this study was conducted in a different subset of neurons, its overarching conclusions regarding molecular mechanism may be generalizable. Another recent publication also demonstrates a role for CLOCK in maintaining synapses (Kobayashi et al., 2015; Musiek et al., 2013). Mice with *Clock* and neuronal PAS domain-containing protein 2 (Npas2) or BMAL1 deletions have synaptic abnormalities. This is consistent with our data in mouse and in human samples. However, a direct connection between CLOCK-mediated transcription and synaptic protein expression has not been defined. CLOCK roles in regulating mitochondrial function and redox mechanisms may also influence neuronal spine formation and maintenance (Kobayashi et al., 2015; Musiek et al., 2013). We demonstrate that CLOCK dysfunction results in defects

in dendritic spines, which may be caused by bioenergetic defects in epileptogenic tissue. These may indirectly affect spine morphology and lead to synaptic defects seen in both the *Emx-Cre; Clock*$^{flox/flox}$ mouse and human focal epilepsy.

The dysregulation of CLOCK and circadian effectors in TSC is particularly interesting because of recent work suggesting interactions between the mTOR and circadian pathways (Lipton et al., 2015). Thus, the circadian and mTOR pathways may interact to exacerbate neuronal dysfunction leading to seizures. In TSC, the mTOR pathway is hyper-activated, and recently published findings demonstrated that the mTOR effector kinase ribosomal S6 kinase (S6K1) phosphorylates and activates BMAL1. This posttranscriptional change shifts the function of BMAL1 to affect protein rather than mRNA synthesis (Lipton et al., 2015). Thus, dysregulation of mTOR activity could impair the function of a critical CLOCK partner, leading to less transcription of downstream effectors, including the PARb ZIP transcription factors. Although BMAL1 level is not altered in human FCD tissue, its function may be altered by dysregulation of the mTOR pathway in TSC. BMAL1 may therefore contribute to epileptogenesis, a hypothesis supported by studies showing that its deletion reduces seizure threshold in mice (Gerstner et al., 2014).

STAR★METHODS

Detailed methods are provided in the online version of this paper and include the following:

CONTACT FOR REAGENT AND RESOURCE SHARING

Further information and requests for resources and reagents should be directed to and will be fulfilled by the Lead Contact, Judy Liu (judy_liu@brown.edu).

EXPERIMENTAL MODEL AND SUBJECT DETAILS

Human Subjects—Patients were enrolled prospectively in our study based on evaluation and subsequent referral by the Comprehensive Program for Pediatric Epilepsy at Children's National Health System or the University of Colorado Pediatric Epilepsy Program for an initial therapeutic resection of an epileptogenic focus. Patients with a primary diagnosis of malignancy were excluded. Informed consent was obtained from parents or guardians of pediatric patients participating in the study (CNHS IRB protocol 5036 or COMIRB Protocol 09-0906) and assent was obtained from pediatric patients when appropriate. Patient demographic information, sex, age of first seizure, medication, as well as the pathological diagnosis were entered into the Study Database. Additional data about pertinent medical history and laboratory results were downloaded from CNHS electronic medical record, including genetic testing, neuroimaging, and EEGs. See Table S1 for patient characteristics. We have not performed the analysis of the influence of gender or other patient characteristic on Clock expression because we only have 8 control samples. Specifically, with regard to sex, we have 6 control specimens from males and only 2 from female patients. No statistical analysis is possible with the limited number of controls. Furthermore, a simple comparison of CLOCK protein levels between male and female patients shows no significant difference $p < 0.8$. Sample sizes for experiments involving human tissue are indicated in Figure

Legends of each experiments and also on Table S1, which states the specific samples that were used in each experiment.

These patients were evaluated according to standard protocols and epileptogenic foci were identified and defined with standard epilepsy protocol imaging by high-resolution 3T MRI and standard intraoperative electrocorticography (ECoG) (Chang et al., 2011). In our surgical cases, the normal tissue that we use as controls for our study was removed in the course of a resection and would have ordinarily been discarded. No normal tissue was ever removed solely for research purposes. In several instances, the normal tissue was collected for our study while no epileptogenic tissue was collected because there was a high clinical suspicion of glioma. In cases with ECoG, the normal tissue control tissue is defined as tissue either beyond the margin of the epileptogenic focus, or tissue underlying grid electrodes without epileptiform discharges.

Mouse Models—Animals were housed in an Association for Assessment and Accreditation of Laboratory Animal Care (AAALAC) accredited facility. All animal care and procedures were carried out in strict accordance with National Institutes of Health Guide for the Care and Use of Laboratory Animals and were approved by the Institutional Animal Care and Use Committee at Children's National Health System (protocol 311-13-11). To obtain *Emx-Cre*; *Clock*$^{flox/flox}$ and *PV-Cre*; *Clock*$^{flox/flox}$ mice, Heterozygous B6.129S4-Clock^{tm1Rep}/J mice (Debruyne et al., 2006) were crossed with *Emx1-Cre*$^{+/-}$ (The Jackson Laboratory, 005628) mice or *PV-Cre*$^{+/-}$ (Hippenmeyer et al., 2005) mice, respectively. All *Emx-Cre; Clock*$^{flox/flox}$, *Emx-Cre control, PV-Cre;Clock*$^{flox/flox}$ and *PV-Cre* control mice are on a C56BL6 background, between ages p21 to p40 were kept in the animal facility with a 12 hour light/12 hour dark cycle, in an enriched environment in cages with no more than 5 animals, before being used for video EEG/pentylenetetrazol (PTZ) seizure induction, whole cell patch-clamp electrophysiology, histological studies, and gene expression studies. These studies were performed in daylight hours between noon and 4pm. We report the sex of mice in the Figure legend in Figure 3. Using two-way ANOVA, to compare male and female conditional Clock mice with male and female mice control mice we did not find differences based on gender on seizure threshold (not shown) for both behavioral and electrographic seizures. Because there was no difference in terms of gender, we performed electrophysiology on male mice. The developmental stage is stated in the figure legends.

Primary Neuronal Cultures—Briefly, mouse cortical neurons were cultured at P0 following papain dissociation using the Worthington papain dissociation system (LK003150, Worthington Biochemical Corporation, Lakewood, NJ). Neurons were plated on polyornithine (Sigma, St. Louis, MO) coated cover glasses in Neurobasal complete (NBC) medium (includes 1% B27, 0.5mM glutamax, 10ng/ml bFGF) (Fu et al., 2013). Briefly, 150,000 neurons were plated on 10mm glass coverslips in 24 well plates and allowed to mature for 13 days.

METHOD DETAILS

Human Tissue

Surgical Sample Collection and Processing: Briefly, for large resections tissue was removed “en bloc.” Bipolar cauterization is used sparingly. Control tissue was collected in the same way as epileptogenic tissue with regard to timing and pathology clearance. Tissue was collected directly from the operating room, within 5 minutes of removal of the tissue from the blood supply and put into oxygenated artificial cerebral spinal fluid (ACSF). Pathology divides the tissue for diagnostic versus research purposes. Upon clearance from pathology, samples were further divided for electrophysiology or storage for later use and then flash frozen directly prior to leaving operating suite on dry ice. Samples were stored at −80 C. No tissue was removed solely for research purposes and control tissue was obtained only when removal was necessary to reach deeper underlying regions of dysplastic/epileptogenetic tissue. All tissue resections occurred between 10:00 AM and noon.

RNA Extraction: Brain tissue samples were subjected to total RNA isolation procedure using Trizol Reagent (Life Technologies, Carlsbad, CA). Concentration of each RNA sample was determined by NanoDrop spectrophotometer ND-1000 (NanoDrop Technologies, Wilmington, DE). The quality of RNA samples was assessed with Agilent 2100 Bioanalyzer (Agilent Technologies Inc., Santa Clara, CA), determining RIN (RNA Integrity Number higher than 6.0).

Microarray: Aliquots of 250ng of high-quality total RNA from each sample was used for the mRNA expression profiling using Illumina Gene Expression BeadChip Array technology (Illumina, Inc., San Diego, CA). First- and second-strand reverse transcription step, followed by a single *in vitro* transcription (IVT) amplification that incorporates biotin-labeled nucleotides, was performed with Illumina TotalPrep −96 RNA Amplification Kit (Ambion, Austin, TX). 750ng of the biotin-labeled IVT product (cRNA) was hybridized to HumanHT-12_v4_BeadChip (Illumina, Inc., San Diego, CA) for 16 hours, followed by washing, blocking, and streptavidin-Cy3 staining according to the Whole-Genome Gene Expression Direct Hybridization protocol (Illumina, Inc., San Diego, CA). The arrays were scanned using HiScanSQ System and obtained decoded images were analyzed by GenomeStudio Gene Expression Module – an integrated platform for the data visualization and analysis (Illumina, Inc., San Diego, CA).

Mouse Model Experiments

Seizure Threshold: Mice from age ranges p30 to p35 were injected with pentylenetetrazol (PTZ) intraperitoneally (IP) at 60 mg/kg. Animals were then video recorded during a 30-minute period and seizures are scored using a modified Racine Seizure scale score ranging from 1-5 (Naydenov et al., 2014). A score of 3 corresponded to a tail twitch and a score of 5 corresponded with tonic-clonic seizures. Assessment of seizure onset and grading of severity was performed by two independent observers blinded to genotype of animals.

Mouse Video EEG: Behavioral, electroencephalogram (Kool et al., 2014), and electromyogram (EMG) observations were made by using the Pinnacle 8400 three channel monitoring system with simultaneous video recording (Pinnacle Technology). Animal

preparation was modified from a previously described method (Arranz et al., 2014). Briefly, adult female and male mice (2 to 4 months old) were anesthetized with Ketamine (100 mg/kg) and Xylazine (5 mg/kg). The skull was exposed with a single incision and all connective tissue was removed. Once the skull was dried four holes were drilled to place 4 sterile stainless-steel screw recording electrodes epidurally (one each placed 0.5-1 mm posterior to bregma in both hemispheres, and one each placed 0.5-1 mm anterior to lambda in both hemispheres. The head-mount and screw recording electrodes were soldered together and secured to the skull with cyanoacrylate. EMG electrodes were implanted in the nuchal muscle. The animals were allowed to recover 5 to 7 days after surgery. For monitoring, a preamplifier was connected to the head-mount and a commutator, which was attached to the Data Acquisition and Control System (Pinnacle Technology). Simultaneous video recording for analysis of the behavior was obtained using Panasonic WV-CP504 video camera connected to a PC. Mice were subjected to 2 hours video-EEG monitoring session consisting of 24 hours baseline measurements and 2 hours measurements post PTZ injection. Alternatively, mice were recorded for 24 hours and then treated with phenobarbital 30 mg/kg via IP injection (Ikegami et al., 2007) and then recorded for another 24 hours. Recordings were sampled at 2kHz and low-pass filtering was done at 100Hz (Kool et al., 2014). EEG signals were collected and analyzed with the Sirenia software package and Excel. Data analysis for spontaneous seizure frequency, seizure onset after PTZ injection, and seizure power spectrums are based on the first 15 minutes acquired during the 2 hours measurements for both baseline and post PTZ injection. EEG signals were rated based on a modified Racine's scoring system (Naydenov et al., 2014): 0 (no response), 1 (freezing), 2 (head nodding or isolated twitches), 3 (orofacial seizures), 4 (clonic seizures), 5 (tonic seizures), and 6 (death). Only abnormal EEG events of grade 1-5 and accompanied with behavioral seizures are included in datasets. Assessment of EEG and video recording was performed after deidentification of the recording with respect to genotype.

Quantitative PCR in Mouse Models: Total RNA was extracted from cortex of 3 control *Emx-Cre; Clock*$^{+/+}$ and 3 *Emx-Cre;Clock*$^{flox/flox}$ mice using TRIzol reagent (Life Technologies) to homogenize tissue, and the Aurum Total RNA Mini Kit (Bio-Rad) to purify samples. cDNA was synthesized using iScript Reverse Transcription Supermix for RT-qPCR (Bio-Rad). The following primers were used to detect PAR-bZIP transcription factors: DBP-`GAGCCTTCTGCAGGGAAACAG` and `GAGTTGCCTTGCGCTCCTTTT`, HLF - `ACGATGGAGAAAATGTCCCG` and `TTTCTTTAC TAAATGCGTCTTCAGG`, and TEF - `CCTTCCCTCTGGTCCTGAAGA` and `CCTTCCCCTTTTCCTTATCGAG`. GAPDH primers are: TTG `ATGGCAACAATCTCCAC` and `CGTCCCGTAGACAAA ATG GT`. Transcript levels were quantified using iTaq Universal SYBR Green Supermix and the CFX connect Real Time System (Bio-Rad).

shRNAi Knockdown of Clock in Primary Neuronal Cultures: We used a bi-cistronic plasmid-based to co-express the shRNA and eGFP previously used in Konishi et al. (2004). We created two Clock knockdown constructs targeting a sequence in the 3′UTR of mouse *Clock* (`CCACAGTTTAAGAGCATCATT`) or coding sequence (`GCACCACCAATAATAGGCTAT`). The corresponded scrambled sequences used as controls are: `CGATCA TAAGGTTTAACCACT` and `ATGCAAAACAGCGTTATCCCA`, respectively (Table S3). The CLOCK expression construct

results in expression of a Flag-tagged mouse CLOCK (Ye et al., 2011). Neurons were transfected using Lipofectamine 2000, as previously described (Fu et al., 2013). Briefly 0.5 μg of DNA in 25 μl of Opti-MEM was combined with 1 μl of Lipofectamine in 25 μl of Opti-MEM for at least 20 minutes at RT to form liposomes. The 50 μl solution was added to coverslips for 2 hours and then exchanged for NBC medium.

On Mouse and Human Samples

Immunocytochemistry/Western Analysis Conditions and Antibodies: For mouse tissue expression studies, at least 3 separate mice were used for each reported result. Mice at P30 were anesthetized with isofluorane, intracardially perfused with 0.1 M PBS (pH 7.4) followed by 4% paraformalde (wt/vol), and the brains were removed and postfixed in 4% paraformaldehyde for 2 hours and transferred to 30% sucrose solution overnight. Coronal tissue sections (20 μm) were cut using a cryostat microtome and collected in PBS. Immunocytochemistry was performed on free-floating sections. Sections were incubated in PBS containing 1% Triton X-100 (vol/vol) for twenty minutes followed by 1 hour incubation in blocking buffer (PBS containing 10% normal goat serum (vol/vol) and 0.5% Triton X-100 (vol/vol)). Sections were incubated with agitation at 4°C overnight in primary antibodies diluted in 0.1 M PBS (pH 7.4). Secondary antibodies were used according to the species of the primary antibodies used: Alexa Fluor 488 or 568-conjugated goat anti-rabbit or anti-mouse IgG (H+L) (ThermoFisher Scientific, A11036, A11031, A10684, A11034, 1:400). Sections were incubated with secondary antibodies and DAPI for 1 h at room temperature followed by PBS washing and mounted on slides using Fluoromount-G (Cat#0100-01, Southern Biotech, Birmingham, AL). Images were acquired using an Olympus FV1000 (Olympus). Images were processed using Photoshop and ImageJ (NIH).

Antiserum against CLOCK (R41) used for immunostaining was obtained from David Weaver (University of Massachussetts, Worchester; LeSauter et al., 2012). Antibodies purchased from Abcam (Cambridge, MA) are: CLOCK (catalog# ab3517, 1:500), which were used for both immunostaining and western blot analysis, Doublecortin (catalog# ab18723, 1:1000), CTIP2 (catalog# ab18465, 1:500), GluR1 (ab31232, 1:1000 dilution) and PSD95 (ab18258 and ab2723, 1:1000). Antibodies for NeuN (catalog# MAB377, 1:200) and BMAL1 (catalog# MAB2298, 1:3000) were obtained from Millipore (Darmstadt, Germany). Antibodies for Brn-2 (catalog# sc-6029, 1:300) and Tubulin-β (catalog# sc-51670, 1:400) were purchased from Santa Cruz Biotechnology Inc. (Dallas, TX). Antibodies for CRY (catalog# CRY11-S, 1:1000) and PER (catalog# PER11-A, 1:1000) were purchased from Alpha Diagnostic International (San Antonio, Texas). Antibodies for Vglut1, Synapsin 1, and VGAT were purchased from Synaptic Systems (catalog# 135304, 106011, and 131011, Goettingen, Germany. Dilutions are 1:1000 for western blotting, 1:500 for immunostaining). Syt2 antibody was from Developmental Studies Hybridoma Bank, Iowa City, Iowa (znp-1). For interneuron staining we used antisera against parvalbumin from SIGMA-ALDRICH (catalog #P3088) and calbindin from SWANT (catalog # 300). To visualize glia we used the GFAP- (Zhuo et al., 1997), and CNP- (Yuan et al., 2002) green fluorescent protein expressing mice.

Western Blot Analysis: Standard Western Blot analysis was performed using antibodies as detailed above. Western blot analysis for human samples detecting CLOCK was repeated three times for each sample. The dual channel signal detection Li-Cor system from Odyssey was used to analyze levels over a linear dynamic range. For the human FCD samples, all tissue samples for which we had enough materials to make protein lysates were tested for CLOCK expression (Table S1) and the reported n in Figure Legends refer to results in separate cases, rather than technical replicates. A subset of cases was tested for CLOCK binding partners and DBP. Control samples for all these expression analyses were run on the same blots as the cases. We always ran the same 5 control cases every time we tested our samples. For BMAL1 the following cases were used: 3, 14, 13, 5, 6, 8, 20, 15, 22, 16. For both PER and CRY, the following cases were tested: 4, 14, 13, 5, 28, 8, 20 and for DBP the following cases were tested: 3, 14, 13, 5, 6, 16, 15,19,10,17. Five cases with decreased CLOCK levels were tested for VGLUT1, Synapsin, Syt2 and VGAT along with 4 control cases.

All antibodies used in immunostaining or western blot analysis have been validated for use in the respective assays and species (see Antibodypedia (https://www.antibodypedia.com/), CiteAb (https://www.citeab.com/).

Electrophysiology Mouse and Human Tissue: Whole cell patch clamp electrophysiology and slice preparation from animals (p25 to p32 from males and females) and human tissue was performed as described previously (Li et al., 2009). Studies were performed in daylight hours between noon and 4pm. Coronal slices of 300μm in thickness were prepared in an ice-cold and oxygenated high-sucrose slicing solution and were then transferred to oxygen-saturated ACSF containing the following (in mM): 126 NaCl, 26 $NaHCO_3$, 10 glucose, 2.5 KCl, 1.25 $NaH_2PO_4.H_2O$, 2 $MgCl_2.6H_2O$, and 2 $CaCl_2$. $2H_2O$; pH 7.4. All slices were incubated at 32°C for one hour prior to recording at room temperature. We followed previously described methods for obtaining electrophysiological parameters for active and passive membrane properties including input resistance, resting membrane potential, capacitance, Rheobase, action potential threshold, amplitude and frequency (Li and Huntsman, 2014).

For spontaneous excitatory postsynaptic currents (sEPSCs), the following intracellular recording solution (in mM) was used: 130 Kgluconate, 10 KCl, 2 MgCl2, 10 HEPES, 10 EGTA, 2 Na2-ATP, 0.5 Na2-GTP. A high chloride intracellular solution was used to study the spontaneous inhibitory postsynaptic currents (sIPSCs) (in mM): 70 Kgluconate, 70 KCl, 2 NaCl, 10 HEPES, 4 EGTA, 2 Na2-ATP, 0.5 Na2-GTP. All recordings were made from Layer 5 of somatosensory cortex. Both sEPSCs and sIPSCs were recorded at −60mV. sIPSCs were recorded in the presence of 20uM DNQX and 100uM DL-AP5 (Tocris Bioscience) to block AMPA and NMDA receptors, respectively. For recording of minature events, 1μMTTX will be applied to the ACSF at the time of recording for both miniature EPSCs or IPSCs. Biocytin (0.5%, Thermo Scientific, Waltham, MA USA) was added to intracellular solutions for post hoc morphological analysis after electrophysiology. All cells were first characterized by action potential firing patterns under current clamp mode and then post synaptic currents (PSCs) were recorded in voltage clamp mode.

All cell-attached recordings were performed at 32°C, and neurons were held at 0pA under voltage clamp mode and high chloride intracellular solution was used, as described above. Action potential frequencies were calculated based on a 75 s period starting from the onset of the third action potential. Recordings were performed using (Multiclamp 700B, Molecular Devices), and digitized (DigiData 1322, Molecular Devices). Measurements of intrinsic and synaptic properties were analyzed offline using Clampfit software (v. 10.2 Molecular Devices).

Morphological Analysis of Mouse and Human Neurons: Biocytin-filled neurons were further processed as previously described (Li and Huntsman, 2014). Images were obtained by confocal microscopy (FluoView, Olympus). Dendritic morphology was quantified by Sholl analysis with ImageJ plugin to place concentric rings centered on the cell soma. Standard dendritic spine analysis was performed as described previously (Sholl, 1953). To minimize bias, images were de-identified first with respect to genotype in mice and control versus epileptogenic tissue for human tissue. Neuronal morphology and spine density were then analyzed by an independent observer.

QUANTIFICATION AND STATISTICAL ANALYSIS

GraphPad Prism was used for the statistical analysis. Shapiro-Wilk's W test was used to test the assumption of normality. For parametric data, the difference between multiple groups was tested by one-way ANOVA. Two-way ANOVA was used when more than two comparisons were made. ANOVA was followed by the Holm-Šídák test. In the case of multiple comparisons of non-parametric data, the Kruskal Wallis test would be used followed by the nonparametric Dunn's post hoc multiple comparisons tests. Comparisons of just two groups were performed with the paired or unpaired Student's t test or the nonparametric Mann–Whitney test, as needed. The level of significance was set at $p < 0.05$. Data are presented as mean ± SEM.

Microarray Bioinformatics—mRNA expression values generated in GenomeStudio were uploaded into the Partek Genomics Suite, version 6.5 (Partek Incorporated, St. Louis, MO) for statistics and data visualization. In Partek, the Robust Multi-array Average (RMA) normalization algorithm was applied to the data, which performed Quantile Normalization, background correction and log2 transformation for the generated expression values. One-way ANOVA statistical test was used for group comparisons, and only expression values with $p < 0.05$ that also survived the step-up False Discovery Rate multiple test adjustment (Benjamini and Hochberg, 1995) were considered for further analyses. As an additional data filter, a 1.5-fold-change expression cut-off was then applied. Partek Venn Diagram tool and Supervised Hierarchical Clustering Analysis, using average linkage algorithm and Euclidean distance metric (2-way clustering) was used for sorting and displaying expression changes that met the above criterion. Ingenuity Pathways Analysis (IPA) software (QIAGEN) was used for pathway analysis and to build networks for putative CLOCK pathways.

General Statistical Analysis of Experiments—Graph Pad Prism was used for the statistical analysis. Shapiro-Wilk's W test was used to test the assumption of normality. For parametric data, the difference between multiple groups was tested by one-way ANOVA.

Two-way ANOVA was used when more than two comparisons were made. ANOVA was followed by the Holm-Šídák test. In the case of multiple comparisons of non-parametric data, the Kruskal Wallis test would be used followed by the nonparametric Dunn's post hoc multiple comparisons tests. Comparisons of just two groups were performed with the paired or unpaired Student's t test or the nonparametric Mann–Whitney test, as needed. The level of significance was set at $p < 0.05$. Data are presented as mean ± SEM. Graphically, error bars represent SEM.

Imaging and Quantification—For colocalization analysis, we imaged the 90×90 μm region of the mouse cortex by using Olympus FV1000 scanning confocal microscope. A z stack for each region was collected (z step of 0.5 μm). At least four regions were imaged for each animal, and three animals were used for each staining. Colocalization of the tested two probes in each section was analyzed using ImageJ plug in Colocalization Threshold under the ImageJ analysis software platform. Pearson's correlation coefficient was used to evaluate the colocalization of the tested two probes.

DATA AND SOFTWARE AVAILABILITY

Microarray Data from Human Surgical Samples—The raw data were deposited at NCBI GEO under project number GEO: GSE62019.

Supplementary Material

Refer to Web version on PubMed Central for supplementary material.

ACKNOWLEDGMENTS

This project was supported by award number UL1TR000075 (J.S.L.) and UL1RR031988 from the NIH National Center for Advancing Translational Sciences. Its contents are solely the responsibility of the authors and do not necessarily represent the official views of the National Center for Advancing Translational Sciences or the National Institutes of Health. J.S.L. and G.V. were funded by a collaborative institutional grant from Children's National Medical Center and Virginia Tech. M.M.H. was funded by NIH R01 NS053719. G.V. was also supported by NIH/NINDS K01NS085071 and NIH/NIA R01 AG055545. N.A.S. was funded by NIH 5T32HD046388. This work was partially supported by the Goldwin Foundation and NIH NCMRR/NINDS 2R24HD050846-06 (NCMRR-DC Core Molecular and Functional Outcome Measures in Rehabilitation Medicine), NIH NCRR UL1RR031988 (GWU-CNMC CTSI), and NIH NICHD (Intellectual and Developmental Disabilities Research Center 1P30HD40677-06). Microscopic analysis at the Children's Research Institute (CRI) Light Microscopy and Image Analysis Core was supported by CRI and NIH grant P30HD040677. M.M.H. was supported by NIH NINDS R01NS095311 and ADR (Associate Dean of Research) Seed Grant University of Colorado, Anschutz Medical Campus. We would like to thank Peter Charles for advice regarding transcriptome analysis, Jason Triplett for help with the manuscript, David Weaver for providing reagents and advice, and Vittorio Gallo for providing support and the CNP- and GFAP-GFP mice.

REFERENCES

Antoch MP, Song EJ, Chang AM, Vitaterna MH, Zhao Y, Wilsbacher LD, Sangoram AM, King DP, Pinto LH, and Takahashi JS (1997). Functional identification of the mouse circadian Clock gene by transgenic BAC rescue. Cell 89, 655–667. [PubMed: 9160756]

Arranz AM, Perkins KL, Irie F, Lewis DP, Hrabe J, Xiao F, Itano N, Kimata K, Hrabetova S, and Yamaguchi Y (2014). Hyaluronan deficiency due to Has3 knock-out causes altered neuronal activity and seizures via reduction in brain extracellular space. J. Neurosci 34, 6164–6176. [PubMed: 24790187]

Benjamini Y, and Hochberg Y (1995). Controlling the false discovery rate: a practical and powerful approach to multiple testing. J. R. Stat. Soc. Ser. A Stat. Soc 57, 289–300.

Blümcke I, Thom M, Aronica E, Armstrong DD, Vinters HV, Palmini A, Jacques TS, Avanzini G, Barkovich AJ, Battaglia G, et al. (2011). The clinicopathologic spectrum of focal cortical dysplasias: a consensus classification proposed by an ad hoc Task Force of the ILAE Diagnostic Methods Commission. Epilepsia 52, 158–174. [PubMed: 21219302]

Bourgeois B (1996). The relationship between sleep and epilepsy in children. Semin. Pediatr. Neurol 3, 29–35. [PubMed: 8795839]

Carreño M, and Fernández S (2016). Sleep-related epilepsy. Curr. Treat. Options Neurol 18, 23. [PubMed: 27059342]

Chang EF, Wang DD, Barkovich AJ, Tihan T, Auguste KI, Sullivan JE, Garcia PA, and Barbaro NM (2011). Predictors of seizure freedom after surgery for malformations of cortical development. Ann. Neurol 70, 151–162. [PubMed: 21761443]

Chattopadhyaya B, Di Cristo G, Higashiyama H, Knott GW, Kuhlman SJ, Welker E, and Huang ZJ (2004). Experience and activity-dependent maturation of perisomatic GABAergic innervation in primary visual cortex during a postnatal critical period. J. Neurosci 24, 9598–9611. [PubMed: 15509747]

Crino PB, Nathanson KL, and Henske EP (2006). The tuberous sclerosis complex. N. Engl. J. Med 355, 1345–1356. [PubMed: 17005952]

D'Gama AM, Geng Y, Couto JA, Martin B, Boyle EA, LaCoursiere CM, Hossain A, Hatem NE, Barry BJ, Kwiatkowski DJ, et al. (2015). Mammalian target of rapamycin pathway mutations cause hemimegalence-phaly and focal cortical dysplasia. Ann. Neurol 77, 720–725. [PubMed: 25599672]

Debruyne JP, Noton E, Lambert CM, Maywood ES, Weaver DR, and Reppert SM (2006). A clock shock: mouse CLOCK is not required for circadian oscillator function. Neuron 50, 465–477. [PubMed: 16675400]

England MJ, Liverman CT, Schultz AM, and Strawbridge LM (2012). Epilepsy across the spectrum: promoting health and understanding. A summary of the Institute of Medicine report. Epilepsy Behav. 25, 266–276. [PubMed: 23041175]

Englot DJ, and Chang EF (2014). Rates and predictors of seizure freedom in resective epilepsy surgery: an update. Neurosurg. Rev 37,389–404, discussion 404–405. [PubMed: 24497269]

Fauser S, Haussler U, Donkels C, Huber S, Nakagawa J, Prinz M, Schulze-Bonhage A, Zentner J, and Haas CA (2013). Disorganization of neocortical lamination in focal cortical dysplasia is brain-region dependent: evidence from layer-specific marker expression. Acta. Neuropathol. Commun 1, 47. [PubMed: 24252438]

Fu X, Brown KJ, Yap CC, Winckler B, Jaiswal JK, and Liu JS (2013). Doublecortin (Dcx) family proteins regulate filamentous actin structure in developing neurons. J. Neurosci 33, 709–721. [PubMed: 23303949]

Gachon F, Fonjallaz P, Damiola F, Gos P, Kodama T, Zakany J, Duboule D, Petit B, Tafti M, and Schibler U (2004). The loss of circadian PAR bZip transcription factors results in epilepsy. Genes Dev. 18, 1397–1412. [PubMed: 15175240]

Gerstner JR, Smith GG, Lenz O, Perron IJ, Buono RJ, and Ferraro TN (2014). BMAL1 controls the diurnal rhythm and set point for electrical seizure threshold in mice. Front. Syst. Neurosci 8, 121. [PubMed: 25018707]

Gorski JA, Talley T, Qiu M, Puelles L, Rubenstein JL, and Jones KR (2002). Cortical excitatory neurons and glia, but not GABAergic neurons, are produced in the Emx1-expressing lineage. J. Neurosci 22, 6309–6314. [PubMed: 12151506]

Hauser WA, Annegers JF, and Kurland LT (1993). Incidence of epilepsy and unprovoked seizures in Rochester, Minnesota: 1935-1984. Epilepsia 34, 453–468. [PubMed: 8504780]

Helbig I, Scheffer IE, Mulley JC, and Berkovic SF (2008). Navigating the channels and beyond: unravelling the genetics of the epilepsies. Lancet Neurol. 7, 231–245. [PubMed: 18275925]

Hesdorffer DC, Logroscino G, Benn EK, Katri N, Cascino G, and Hauser WA (2011). Estimating risk for developing epilepsy: a population-based study in Rochester, Minnesota. Neurology 76, 23–27. [PubMed: 21205691]

Hippenmeyer S, Vrieseling E, Sigrist M, Portmann T, Laengle C, Ladle BR, and Arber S (2005). A developmental switch in the response of DRG neurons to ETS transcription factor signaling. PLoS Biol. 3, e159. [PubMed: 15836427]

Ikegami K, Heier RL, Taruishi M, Takagi H, Mukai M, Shimma S, Taira S, Hatanaka K, Morone N, Yao I, et al. (2007). Loss of alpha-tubulin polyglutamylation in ROSA22 mice is associated with abnormal targeting of KIF1A and modulated synaptic function. Proc. Natl. Acad. Sci. USA 104, 3213–3218. [PubMed: 17360631]

Jansen LA, Mirzaa GM, Ishak GE, O'Roak BJ, Hiatt JB, Roden WH, Gunter SA, Christian SL, Collins S, Adams C, et al. (2015). PI3K/AKT pathway mutations cause a spectrum of brain malformations from megalence-phaly to focal cortical dysplasia. Brain 138, 1613–1628. [PubMed: 25722288]

Jin X, Huguenard JR, and Prince DA (2011). Reorganization of inhibitory synaptic circuits in rodent chronically injured epileptogenic neocortex. Cereb. Cortex 21, 1094–1104. [PubMed: 20855494]

King DP, Zhao Y, Sangoram AM, Wilsbacher LD, Tanaka M, Antoch MP, Steeves TD, Vitaterna MH, Kornhauser JM, Lowrey PL, et al. (1997). Positional cloning of the mouse circadian clock gene. Cell 89, 641–653. [PubMed: 9160755]

Kobayashi Y, Ye Z, and Hensch TK (2015). Clock genes control cortical critical period timing. Neuron 86, 264–275. [PubMed: 25801703]

Konishi Y, StegmCiüer J, Matsuda T, Bonni S, and Bonni A (2004). Cdh1-APC controls axonal growth and patterning in the mammalian brain. Science 303, 1026–1030. [PubMed: 14716021]

Kool M, Jones DT, Jäger N, Northcott PA, Pugh TJ, Hovestadt V, Piro RM, Esparza LA, Markant SL, Remke M, et al.; ICGC PedBrain Tumor Project (2014). Genome sequencing of SHH medulloblastoma predicts genotype-related response to smoothened inhibition. Cancer Cell 25, 393–405. [PubMed: 24651015]

Krook-Magnuson EI, Li P, Paluszkiewicz SM, and Huntsman MM (2008). Tonically active inhibition selectively controls feedforward circuits in mouse barrel cortex. J. Neurophysiol 100, 932–944. [PubMed: 18509076]

Kuhlman SJ, Olivas ND, Tring E, Ikrar T, Xu X, and Trachtenberg JT (2013). A disinhibitory microcircuit initiates critical-period plasticity in the visual cortex. Nature 501, 543–546. [PubMed: 23975100]

Lerche H, Shah M, Beck H, Noebels J, Johnston D, and Vincent A (2013). Ion channels in genetic and acquired forms of epilepsy. J. Physiol 591, 753–764. [PubMed: 23090947]

Lerner JT, Salamon N, Hauptman JS, Velasco TR, Hemb M, Wu JY, Sankar R, Donald Shields W, Engel J, Jr., Fried I, et al. (2009). Assessment and surgical outcomes for mild type I and severe type II cortical dysplasia: a critical review and the UCLA experience. Epilepsia 50, 1310–1335. [PubMed: 19175385]

LeSauter J, Lambert CM, Robotham MR, Model Z, Silver R, and Weaver DR (2012). Antibodies for assessing circadian clock proteins in the rodent suprachiasmatic nucleus. PLoS ONE 7, e35938. [PubMed: 22558277]

Li P, and Huntsman MM (2014). Two functional inhibitory circuits are comprised of a heterogeneous population of fast-spiking cortical interneurons. Neuroscience 265, 60–71. [PubMed: 24480365]

Li P, Rudolph U, and Huntsman MM (2009). Long-term sensory deprivation selectively rearranges functional inhibitory circuits in mouse barrel cortex. Proc. Natl. Acad. Sci. USA 106, 12156–12161. [PubMed: 19584253]

Lipton JO, Yuan ED, Boyle LM, Ebrahimi-Fakhari D, Kwiatkowski E, Nathan A, Güttler T, Davis F, Asara JM, and Sahin M (2015). The circadian protein BMAL1 regulates translation in response to S6K1-mediated phosphorylation. Cell 161, 1138–1151. [PubMed: 25981667]

Mantegazza M, Rusconi R, Scalmani P, Avanzini G, and Franceschetti S (2010). Epileptogenic ion channel mutations: from bedside to bench and, hopefully, back again. Epilepsy Res. 92, 1–29. [PubMed: 20828990]

Micheva KD, Busse B, Weiler NC, O'Rourke N, and Smith SJ (2010). Single-synapse analysis of a diverse synapse population: proteomic imaging methods and markers. Neuron 68, 639–653. [PubMed: 21092855]

Morey JS, Ryan JC, and Van Dolah FM (2006). Microarray validation: factors influencing correlation between oligonucleotide microarrays and real-time PCR. Biol. Proced. Online 8, 175–193. [PubMed: 17242735]

Muhlebner A, Iyer AM, van Scheppingen J, Anink JJ, Jansen FE, Veersema TJ, Braun KP, Spliet WG, van Hecke W, Soylemezoglu F, et al. (2016). Specific pattern of maturation and differentiation in the formation of cortical tubers in tuberous sclerosis omplex (TSC): evidence from layer-specific marker expression. J. Neurodev. Disord 8, 9. [PubMed: 27042238]

Musiek ES, Lim MM, Yang G, Bauer AQ, Qi L, Lee Y, Roh JH, Ortiz- Gonzalez X, Dearborn JT, Culver JP, et al. (2013). Circadian clock proteins regulate neuronal redox homeostasis and neurodegeneration. J. Clin. Invest 123, 5389–5400. [PubMed: 24270424]

Narayanan V (2003). Tuberous sclerosis complex: genetics to pathogenesis. Pediatr. Neurol 29, 404–409. [PubMed: 14684235]

Naydenov AV, Horne EA, Cheah CS, Swinney K, Hsu KL, Cao JK, Marrs W, Blankman JL, Tu S, Cherry AE, et al. (2014). ABHD6 blockade exerts antiepileptic activity in PTZ-induced seizures and in spontaneous seizures in R6/2 mice. Neuron 83, 361–371. [PubMed: 25033180]

Paz JT, and Huguenard JR (2015). Microcircuits and their interactions in epilepsy: is the focus out of focus? Nat. Neurosci 18, 351–359. [PubMed: 25710837]

Scheffer IE, Heron SE, Regan BM, Mandelstam S, Crompton DE, Hodgson BL, Licchetta L, Provini F, Bisulli F, Vadlamudi L, et al. (2014). Mutations in mammalian target of rapamycin regulator DEPDC5 cause focal epilepsy with brain malformations. Ann. Neurol 75, 782–787. [PubMed: 24585383]

Sommeijer JP, and Levelt CN (2012). Synaptotagmin-2 is a reliable marker for parvalbumin positive inhibitory boutons in the mouse visual cortex. PLoS One 7, e35323. [PubMed: 22539967]

Sholl DA (1953). Dendritic organization in the neurons of the visual and motor cortices of the cat. J. Anat 87, 387–406. [PubMed: 13117757]

Tavazoie SF, Alvarez VA, Ridenour DA, Kwiatkowski DJ, and Sabatini BL (2005). Regulation of neuronal morphology and function by the tumor suppressors Tsc1 and Tsc2. Nat. Neurosci 8, 1727–1734. [PubMed: 16286931]

Thom M, Martinian L, Sen A, Cross JH, Harding BN, and Sisodiya SM (2005). Cortical neuronal densities and lamination in focal cortical dysplasia. Acta. Neuropathol 110, 383–392. [PubMed: 16151726]

Trettel J, and Levine ES (2003). Endocannabinoids mediate rapid retrograde signaling at interneuron right-arrow pyramidal neuron synapses of the neocortex. J. Neurophysiol 89, 2334–2338. [PubMed: 12686587]

Wong M (2013). Mammalian target of rapamycin (mTOR) activation in focal cortical dysplasia and related focal cortical malformations. Exp. Neurol 244, 22–26. [PubMed: 22015915]

Ye R, Selby CP, Ozturk N, Annayev Y, and Sancar A (2011). Biochemical analysis of the canonical model for the mammalian circadian clock. J. Biol. Chem 286, 25891–25902. [PubMed: 21613214]

Yuan X, Chittajallu R, Belachew S, Anderson S, McBain CJ, and Gallo V (2002). Expression of the green fluorescent protein in the oligodendrocyte lineage: a transgenic mouse for developmental and physiological studies. J. Neurosci. Res 70, 529–545. [PubMed: 12404507]

Zeng LH, Xu L, Gutmann DH, and Wong M (2008). Rapamycin prevents epilepsy in a mouse model of tuberous sclerosis complex. Ann. Neurol 63, 444–453. [PubMed: 18389497]

Zhuo L, Sun B, Zhang CL, Fine A, Chiu SY, and Messing A (1997). Live astrocytes visualized by green fluorescent protein in transgenic mice. Dev. Biol 187, 36–42. [PubMed: 9224672]

Highlights

- CLOCK transcription factor expression is low in human epileptogenic brain tissue
- Deletion of *Clock* in pyramidal cells causes seizures during sleep in mice
- Inhibition of CLOCK-deficient pyramidal cells in mouse and human is diminished

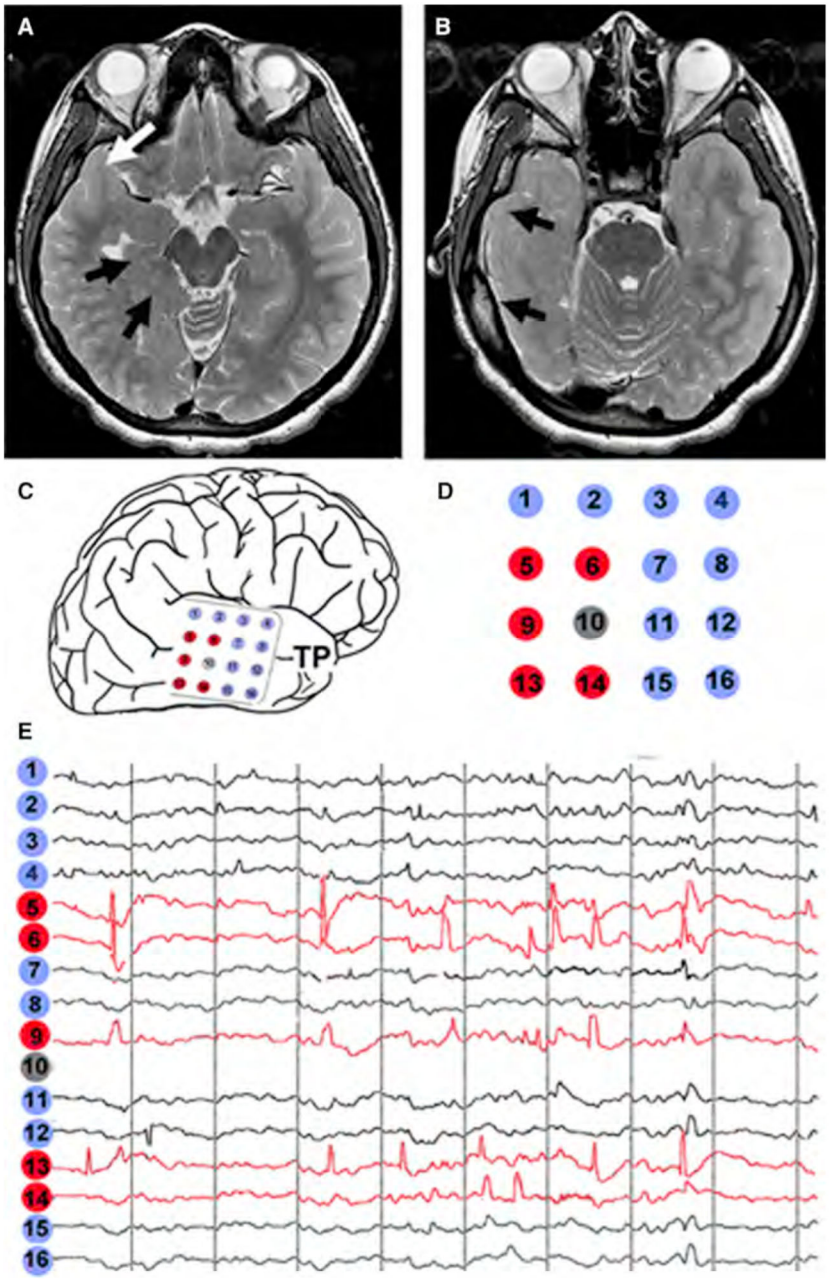

Figure 1. The Epileptogenic Focus Is Defined in a Patient Undergoing Resection

T2 weighted MRI images of a patient (case 1) with a right temporal dysplasia are shown.

(A)The pre-surgical MRI shows dysplasia involving the right mesial temporal lobe (black arrows) with a normal temporal tip (white arrow) is shown.

(B)On an inferior cut of the MRI from the same patient, the dysplasia extends out to the surface of the temporal lobe (black arrows).

(C)This panel shows the diagram of grid placement over the surface of the temporal lobe prior to resection with its orientation to the temporal pole.

(D)The higher power diagram of the grid shows the numbering of the electrodes. Blue electrodes correspond to leads with normal tracings, and the red electrodes are in positions with epileptiform discharges, as shown in the subsequent panel.
(E)The electrocorticography (ECoG) demonstrates frequent spike-and-wave discharges at the right posterior temporal lobe in leads 5, 6, 9, 13, and 14 (red). The lead at position 10 did not contact the cortical surface, while other leads (blue) did not demonstrate epileptiform discharges. In this case, the superior temporal gyrus and temporal tip were removed to reach the focus and these regions were used as control samples.

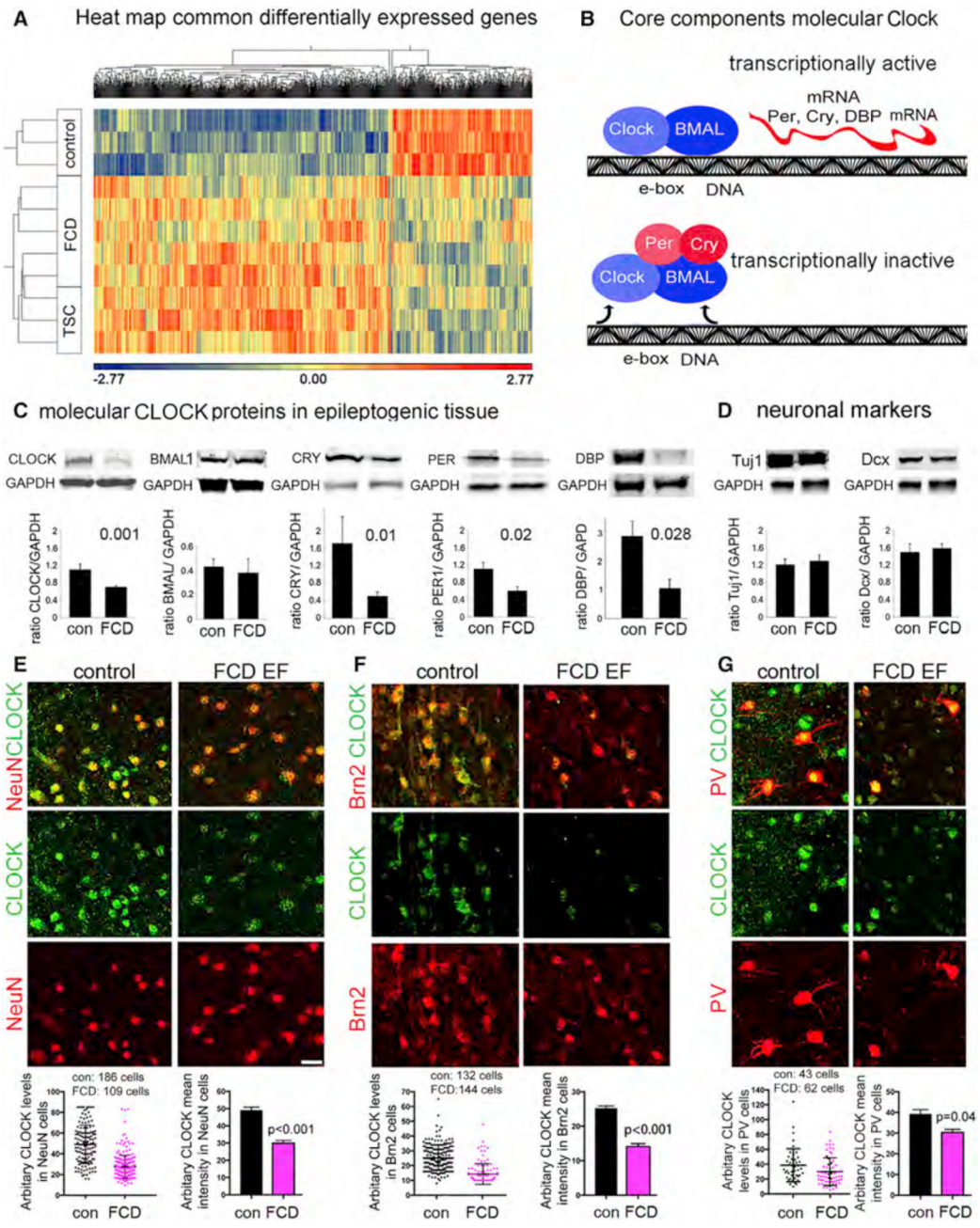

Figure 2. CLOCK Is Reduced in Human Epileptogenic Tissue

(A)Gene expression in human epileptogenic tissue: using microarray, we compared control tissue, tissue from FCD cases, and tissue from TSC surgical cases. Prior to application of FDR, expression of 900 genes is changed in the same way in FCD and TSC, as compared to control tissue. The heatmap shows expression changes that are common to both in FCD and TSC cases versus control with red denoting upregulation and blue downregulation of expression levels. See also Figure S1 and Table S1.

(B)Diagram of the core components of the circadian molecular clock: CLOCK is a transcription factor that dimerizes with BMAL1 to bind to E-box elements in promoters of

their target genes, including repressors of CLOCK/BMAL1 transcription, the PER and CRY proteins, and other downstream targets, such as DBP. CRY and PER proteins bind to CLOCK/BMAL1 to inhibit its transcriptional activity.

(C)Western analysis of the core components of the circadian molecular CLOCK demonstrates decreased CLOCK in epileptogenic FCD tissue as compared to non-epileptogenic controls. The graphs show pooled data from controls (con, n = 5) and the FCD tissue (n = 18) that we tested for CLOCK expression. Decrease of CLOCK and CLOCK downstream target gene products: CRY (n = 7), PER1 (n = 7), and DBP (n= 10) are statistically significant in FCD, in contrast to BMAL1, which is unchanged in epileptogenic tissue (n = 10). See also Figure S2A.

(D)In the same samples, we find that neuronal markers TUJ1 and doublecortin (DCX) are not significantly changed.

(E–G) In control human tissue, CLOCK co-localizes with the neuronal marker NeuN (E), Brn2 (F), and PV (G), respectively. The panels are representative staining results from three control tissue and three FCD samples. Arbitrary CLOCK intensity in each NeuN-positive, Brn2-positive, and PV-positive cells is compared between controls (con) and epileptogenic tissues (FCD). The numbers of cells counted are shown on the top of the panels located at the bottom of each representative immunostaining pictures. The average CLOCK intensity is also calculated. Loss of CLOCK expression is significant in both NeuN-positive and Brn2-positive neurons of epileptogenic tissues (FCD) compared to controls. CLOCK is decreased in some of the PARV-positive neurons in the epileptogenic focus. Scale bar represents 20 μm for (E)–(G). All significant p values (less than 0.05) calculated by two-tailed t test are shown on the graphs. Error bars represent SEM. See also Figures S1 and S2 and Tables S1 and S2.

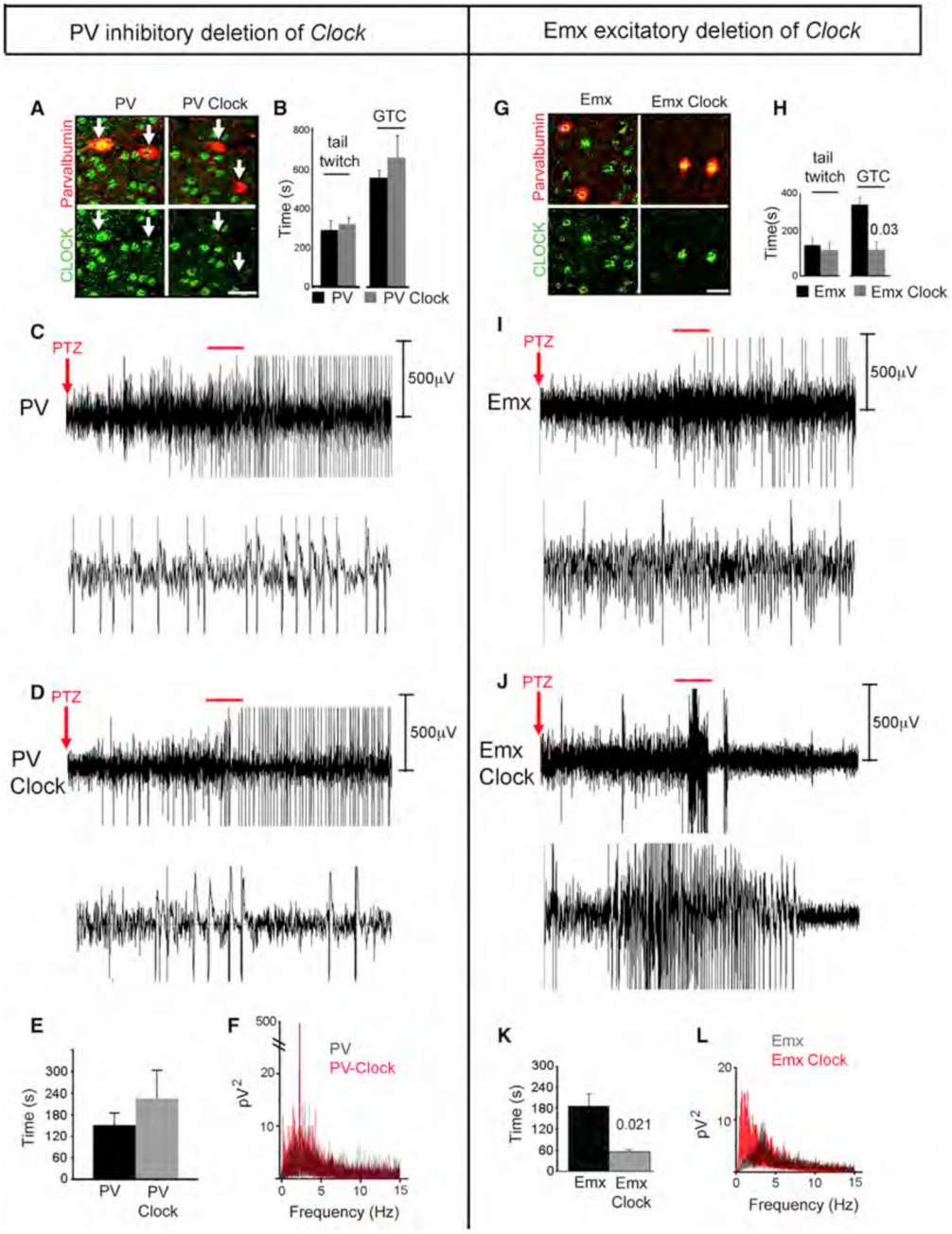

Figure 3. Selective Deletion of *Clock* in Pyramidal Neurons Results in Decreased Seizure Threshold

(A)In *PV-Cre; Clock*$^{flox/flox}$ mice, CLOCK (green) is not detected in parvalbumin (PV)-positive interneurons (red) but is preserved in other cells.

(B)Seizure threshold in *PV-Cre; Clock*$^{flox/flox}$ mice (n = 15 with 7 females and 8 males) is not significantly different from the control *PV-Cre* mice (n = 8 with 4 females and 4 males).

(C and D) EEG recording of the response following pentylenetetrazol (PTZ) is shown in a representative *PV-Cre* mouse (C) and a *PV-Cre; Clock*$^{flox/flox}$ (D) mouse, respectively. The top panels show the first 5 min after PTZ, and the expanded 30 s EEG trace of the region indicated by the red line is shown on the lower panels.

(E)Histogram comparing mean latency of seizure onset as measured by video EEG after PTZ administration.

(F)Average EEG power spectrum of the first 15 min after PTZ administration for *PV-Cre* (black) and *PV-Cre; Clock*$^{flox/flox}$ (red) mice is shown. For the video-EEG experiments, n = 6 with 3 females and 3 males for *PV-Cre* controls and n = 7 for *PV-Cre; Clock*$^{flox/flox}$ mice with 3 females and 4 males.

(G)The *Emx-Cre; Clock*$^{flox/flox}$ mouse cortex is immunostained with CLOCK (green) and PV (red). *Clock* expression is preserved in PV-expressing interneurons, while it is absent in many other neurons. See also Figure S3.

(H)*Emx-Cre; Clock*$^{flox/flox}$ mice (n = 9 with 6 males and 3 females) have a decreased latency to generalized tonic-clonic seizures (GTC) as compared with *Emx-Cre* controls (n = 19 with 9 males and 10 females) following PTZ treatment, as measured by modified Racine scale. Data were analyzed using ANOVA.

(I and J) A 5 min EEG trace of the response following PTZ is shown in a representative *Emx-Cre* control mouse (I) as compared to an *Emx-Cre; Clock*$^{flox/flox}$ mouse (J). The bottom panels in both (I) and (J) show an expanded view of the 30 s trace (highlighted with red lines in the top panels). The increased discharges in EEG are observed from *Emx-Cre; Clock*$^{flox/flox}$ mouse.

(K)Histogram comparing mean latency of seizure onset after PTZ administration demonstrates a significantly reduced latency to high-amplitude epileptiform discharges in *Emx-Cre; Clock*$^{flox/flox}$ mice as compared to *Emx-Cre* control mice.

(L)Average EEG power spectrum of the first 15 min after PTZ administration for *Emx-Cre* (black) and *Emx-Cre; Clock*$^{flox/flox}$ (red) mice is shown. All significant p values (less than 0.05) calculated by two-tailed t test are shown on the graphs. For the video-EEG experiments, n = 6 with 3 females and 3 males for *Emx-Cre* controls and n = 6 for *Emx-Cre; Clock*$^{flox/flox}$ mice with 3 females and 3 males. All significant p values (less than 0.05) calculated by two-tailed t test are shown on the graphs. Error bars represent SEM. See also Figure S3.

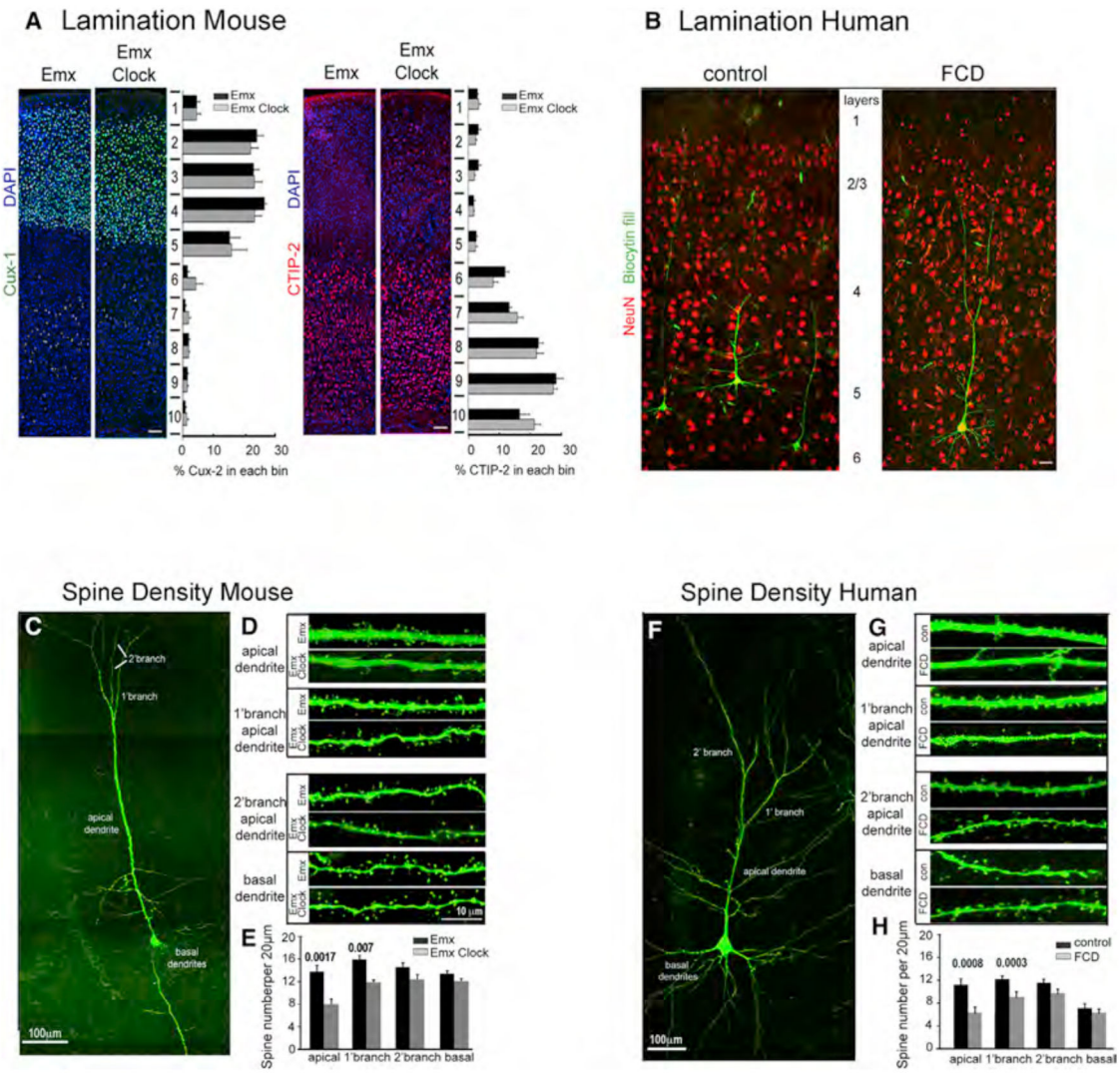

Figure 4. *Emx-Cre; Clock*$^{flox/flox}$ Mice Have No Laminar Defects but Exhibit Specific Spine Defects Similar to Epileptogenic Tissue

(A)The laminar distribution of somatosensory cortical neurons positive for Cux1, an upper layer marker (II-IV), and for CTIP2, a layer 5 marker. is normal in *Emx-Cre; Clock*$^{flox/flox}$ mice. The percentage of positive neurons in ten equal regions of the cortex spanning pial surface to the ventricular zone of the cortex is counted and compared between control *Emx-Cre* and *Emx-Cre; Clock*$^{flox/flox}$ mice. Differences are calculated by the chi-square test. Scale bar represents 50 μm.

(B)In contrast, lamination is highly variable in tissue comprising the epileptogenic focus from FCD cases, as determined by staining with the neuronal marker NeuN (red). The green channel shows the morphology of neurons that have been filled with biocytin during whole-cell recording. Scale bar represents 20 μm.

(C)The image of a biocytin-filled layer 5 cortical pyramidal neuron from somatosensory cortex region of a control *Emx-Cre* mouse, with its dendrites labeled as: apical, 1′ branch, 2′ branch, and basal dendrites.

(D)High-power views of representative dendritic regions are shown for both *Emx-Cre* control (Emx) (31 cells from 9 mice) and *Emx-Cre; Clock*$^{flox/flox}$ (Emx Clock) (18 cells from 7 mice) neurons.
(E)Measurement of dendritic spine density demonstrates significant decreases in the apical dendrite and the 1′ branches.
(F)A pyramidal neuron from human control tissue is shown (biocytin filled). The dendrites are labeled: apical, 1′ branch, 2′ branch, and basal dendrites.
(G)High-power views of representative dendritic regions are shown for both control tissue (con) and epileptogenic tissue from patients with FCD (FCD).
(H)Measurement of dendritic spine density demonstrates significant decreases in the apical dendrite and the 1′ branches in 5 cases of FCD (n = 23 neurons) (Table S1) versus neurons in control tissue (n = 21 neurons from 4 individual patients). All significant p values (less than 0.05) calculated by two-tailed t test are shown on the graphs. Error bars represent SEM. See also Figure S4 and Tables S2 and S3.

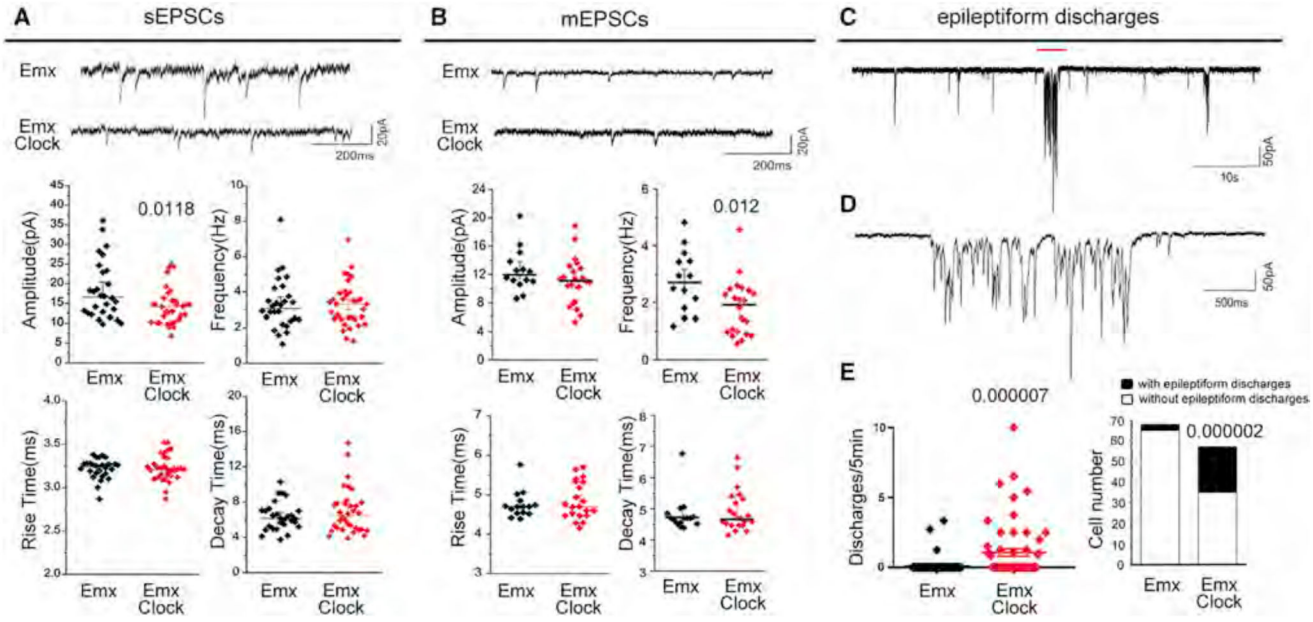

Figure 5. Spontaneous Excitatory Postsynaptic Currents Recordings Reveal Epileptiform Discharges in *Emx-Cre; Clock*$^{flox/flox}$ Pyramidal Neurons

(A)Spontaneous excitatory postsynaptic currents (sEPSCs) are altered in *Emx-Cre; Clock*$^{flox/flox}$ mice. Representative raw traces of sEPSCs recorded under voltage-clamp mode are shown for control (Emx) and *Emx-Cre; Clock*$^{flox/flox}$ (Emx CLOCK) L5 pyramidal neurons. Analysis of recordings show sEPSC amplitude is significantly different between control (n = 28 neurons from 13 mice) and *Emx-Cre; Clock*$^{flox/flox}$ pyramidal neurons (n = 34 neurons from 14 mice), while there is no significant difference in sEPSC frequency, rise time, or decay time between control and *Clock*-deficient pyramidal neurons.

(B)Miniature excitatory post synaptic currents (mEPSCs) are decreased in frequency in L5 pyramidal neurons (n = 22 from 5 *Emx-Cre; Clock*$^{flox/flox}$ mice) compared with *Emx-Cre* controls (n = 14 neurons from 4 mice). sEPSCs were recorded at −60 mV with physiological intracellular solution (130 mM Kgluconate, 10 mM KCl). The recording of mEPSCs was performed in the presence of 1 μM TTX. Significant p values calculated by two-tailed t test are shown.

(C)Poly-spike epileptiform activity is observed in the raw trace of sEPSCs recorded from an *Emx-Cre; Clock*$^{flox/flox}$ pyramidal neuron.

(D)The expanded view of one segment of the trace marked by a red line in (C) is shown.

(E)Left: scatterplot of the occurrence of epileptiform discharges per 5 min. Horizontal bars within the plot show mean values. Significant p values (less than 0.05) calculated by Mann-Whitney test. Right: comparison of cell numbers in *Emx-Cre* and *Emx-Cre; Clock*$^{flox/flox}$ exhibiting epileptiform discharges. Black bars represent the proportion of cells with epileptiform discharges. Fisher's exact test was used to demonstrate significance. See also Figure S5.

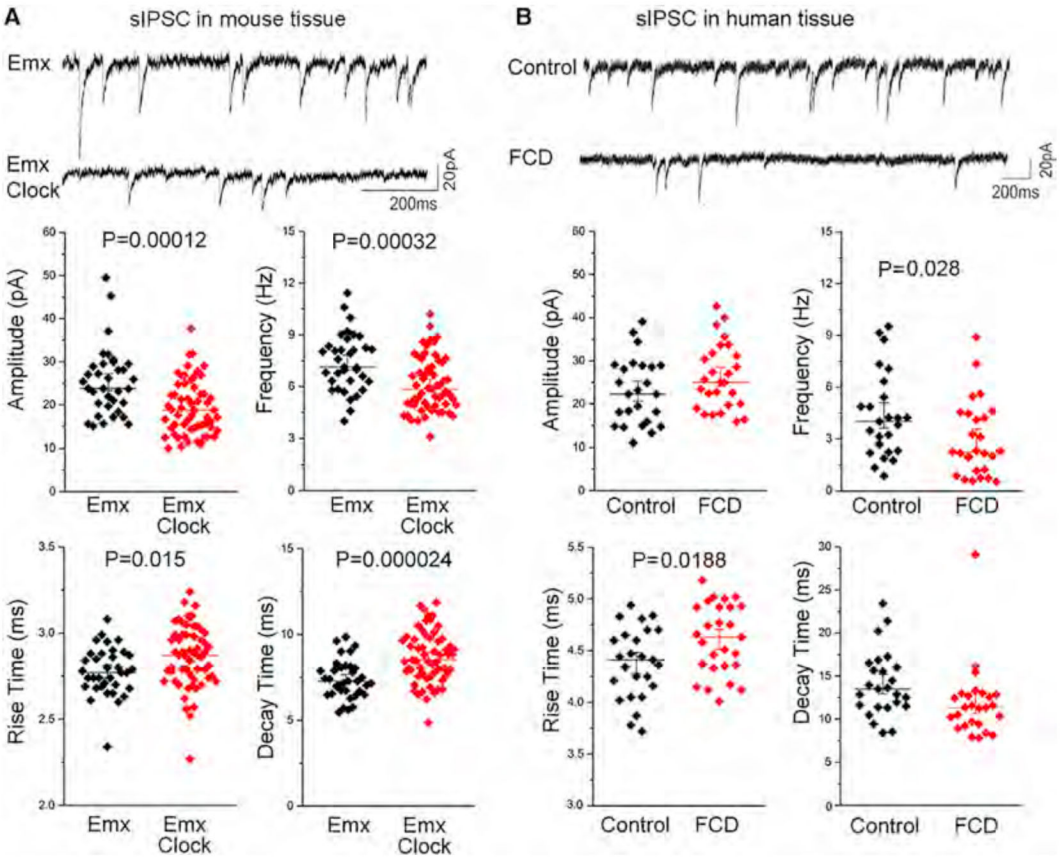

Figure 6. Significant Defects Were Observed in Spontaneous Inhibitory Postsynaptic Currents in Pyramidal Neurons from *Emx-Cre; Clock*$^{flox/flox}$ Mice and Human Epileptogenic Tissue

(A)Representative raw traces of spontaneous inhibitory postsynaptic currents (sIPSCs) from *Emx-cre* and *Emx-cre Clock*$^{flox/flox}$ pyramidal neurons are shown. sIPSC amplitude, frequency, rise time, and decay time are significantly changed in CLOCK-deficient neurons (n = 58 from 21 mice) as compared with control (n = 35 from 11 mice).

(B)We examined sIPSCs in pyramidal neurons from human FCD epileptogenic tissues. We find a defect in the frequency and rise time of sIPSCs in epileptogenic FCD cases (27 neurons from 5 cases) compared with neurons from control tissue (25 neurons from 3 cases). Cells were held at −60 mV during recording, and high chloride (70 mM Kgluconate, 70 mM KCl) was used for sIPSC recordings, with 20 μM DNQX and 100 μM DL-AP5 to block AMPA and NMDA receptors, respectively. Significant p values (less than 0.05) calculated by two-tailed t test are shown on the graphs. See also Figure S6 and Tables S2 and S4.

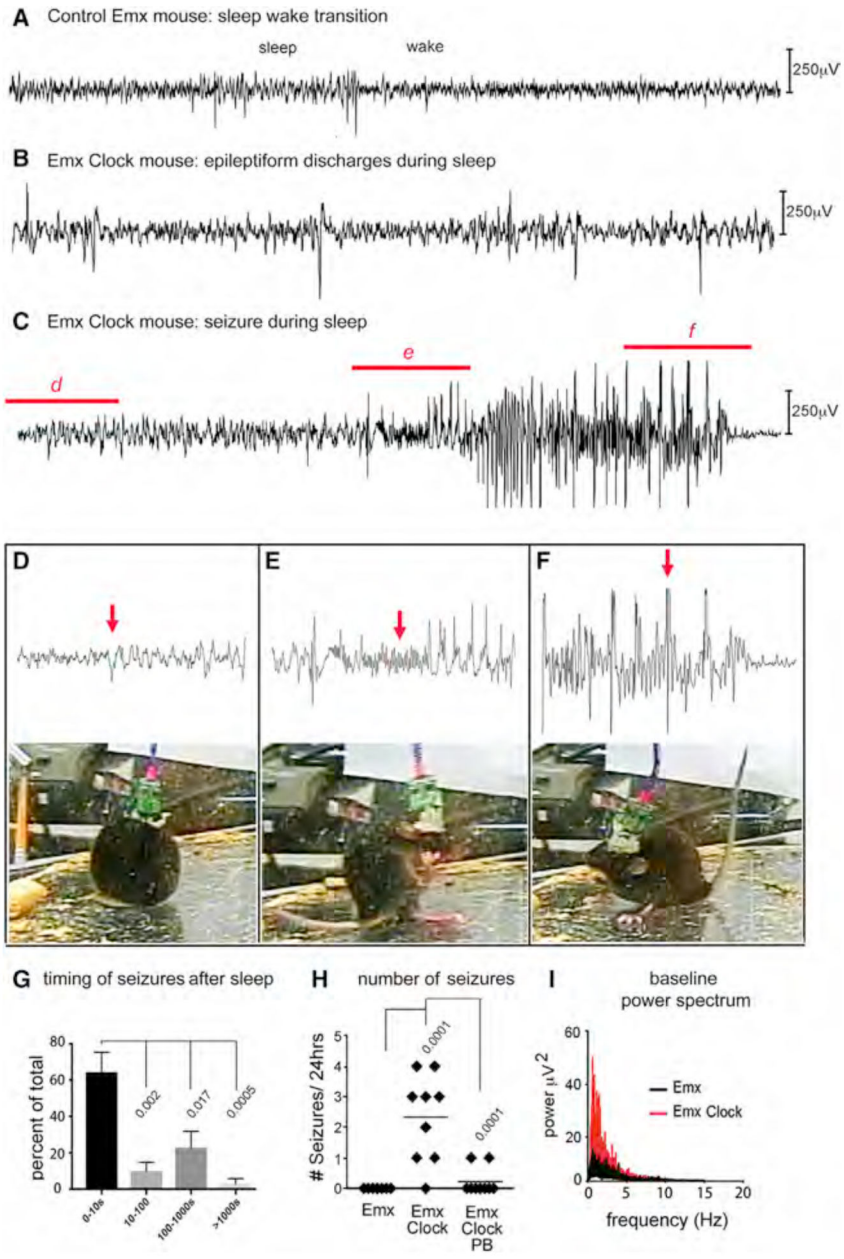

Figure 7. Spontaneous Seizures in *Emx-Cre; Clock*$^{flox/flox}$ Mice Are Related to Sleep

(A) Baseline video EEG of a control *Emx-cre* (Emx) mouse demonstrates a normal transition from sleep to wakefulness. A 30 s trace is shown.

(B) Panel shows a 30 s EEG trace of epileptiform discharges in sleep from an *Emx-Cre; Clock*$^{flox/flox}$ (Emx Clock) mouse. See Movie S1.

(C) A spontaneous seizure (Racine grade 5) arises from sleep in an *Emx-Cre; Clock*$^{flox/flox}$ mouse. See Movie S2.

(D-F) Expanded 5 s traces of EEG from regions indicated in (C) are shown with a frame from the video recording taken at the time point shown with red arrows. The EEG trace is obtained from onset of sharp activity from sleep is shown (D). The video shows a sleeping mouse. The trace is taken from the start of the behavioral seizure and increased EMG

activity with fast activity following a generalized spike-wave complex (E). The arrow shows the region of the EEG, which corresponds the video panel showing the mouse rearing/falling. The trace shows the resolution of the seizure (F). The EEG shows spike-wave complexes followed by postictal depression. Video panel shows the mouse with its tail in a tonic position.

(G)The timing of seizures after EEG recording of sleep is shown. Seizures from eight *Emx-Cre; Clock*$^{flox/flox}$ mice are binned according to their onset after the end of sleep. Bins are of increasing sizes: 0–10 s, 10–100 s, 100–1,000 s, and >1,000 s. Approximately 60% of seizures occur within 10 s of SWS. A two-way ANOVA analysis was used to demonstrate significance. 32 seizures were detected and used in this analysis.

(H)Histogram comparing the mean frequency of spontaneous seizures between *Emx-cre* and *Emx-Cre; Clock*$^{flox/flox}$ mice shows that *Emx-Cre* mice have no observable seizures in contrast to spontaneous seizures in *Emx-Cre; Clock*$^{flox/flox}$ mice. Injecting *Emx-Cre; Clock*$^{flox/flox}$ mice with 30 mg/kg of phenobarbital (Emx Clock PB) results in a statistically significant reduction in seizures in the subsequent 24-hr period. Significant p values (less than 0.05) calculated by two-tailed t test are shown on the graphs (n = 8 mice in each group). Error bars represent SEM.

(I)Average baseline EEG power spectrum of *Emx-Cre; Clock*$^{flox/flox}$ (red) and control *Emx-Cre* (black) mice compares the mean power versus frequencies and shows higher amplitudes in the *Emx-Cre; Clock*$^{flox/flox}$ mice (n = 4) versus *Emx-Cre* control (n = 6). Also see Figure S7.

KEY RESOURCES TABLE

REAGENT or RESOURCE	SOURCE	IDENTIFIER
Antibodies		
Rabbit anti-Clock	LeSauter et al., 2012	N/A
Rabbit anti-Clock	Abcam	Abcam Cat# ab3517; RRID: AB_303866
Rabbit anti-Doublecortin	Abcam	Abcam Cat# ab18723; RRID: AB_732011
Rat anti-CTIP2	Abcam	Abcam Cat# ab18465; RRID: AB_10015215
Rabbit anti-GluR1	Abcam	Abcam Cat# ab31232; RRID: AB_2113447
Rabbit anti-PSD95	Abcam	Abcam Cat# ab18258; RRID: AB_444362
Mouse anti-PSD95	Abcam	Abcam Cat# ab2723; RRID: AB_303248
Mouse anti-NeuN	Millipore	Millipore Cat# MAB377; RRID: AB_2298772
Rabbit anti-BMAL1	Millipore	Cat# MAB2298
Goat anti-Brn-2	Santa Cruz Biotechnology	Santa Cruz Biotechnology Cat# sc-6029; RRID: AB_2167385
Mouse anti-Tubulin-β	Santa Cruz Biotechnology	Santa Cruz Biotechnology Cat# sc-51670; RRID: AB_630408
Rabbit anti-CRY	Alpha Diagnostic International	Alpha Diagnostic International Cat# CRY11-A; RRID: AB_1614505
Rabbit anti-PER	Alpha Diagnostic International	Alpha Diagnostic International Cat# PER11-A; RRID: AB_1620949
Pig anti-Vglut1	Synaptic Systems	Synaptic Systems Cat# 135 304; RRID: AB_887878
Mouse anti-Synapsin 1	Synaptic Systems	Synaptic Systems Cat# 106 011; RRID: AB_2619772
Mouse anti-VGAT	Synaptic Systems	Synaptic Systems Cat# 131 011; RRID: AB_887872
Mouse anti-Syt2	Developmental Studies Hybridoma Bank	DSHB Cat# znp-1; RRID: AB_2315626
Mouse anti-parvalbumin	Sigma-Aldrich	Sigma-Aldrich Cat# P3088; RRID: AB_477329
Mouse anti-Calbindin	SWANT	Swant Cat# 300; RRID: AB_10000347
Alexa 488-conjugated goat anti-rabbit IgG (H+L)	Thermo Fisher Scientific	Cat# A11036 Thermo Fisher Scientific Cat# A32731; RRID: AB_2633280
Alexa 568-conjugated goat anti-rabbit IgG (H+L)	Thermo Fisher Scientific	Thermo Fisher Scientific Cat# A-11036 also A11036; RRID: AB_10563566
Alexa 488-conjugated goat anti-mouse IgG (H+L)	Thermo Fisher Scientific	Thermo Fisher Scientific Cat# A32723; RRID: AB_2633275
Alexa 568-conjugated goat anti-mouse IgG (H+L)	Thermo Fisher Scientific	Thermo Fisher Scientific Cat# A-11031; RRID: AB_144696
Chemicals, Peptides, and Recombinant Proteins		

REAGENT or RESOURCE	SOURCE	IDENTIFIER
Pentylenetetrazol (PTZ)	Sigma-Aldrich	P6500-25G
Lipofectamine 2000	Thermo Fisher Scientific	Cat# 11668019
Polyornithine	Sigma-Aldrich	Cat# P4957-50ML
B27	Thermo Fisher Scientific	Cat# 17504044
bFGF	Thermo Fisher Scientific	Cat# PHG0024
Trizol Reagent	Life Technologies	Cat# 15596018
Ketamine	Sigma-Aldrich	Cat# K-002
Xylazine	Sigma-Aldrich	Cat# 32555
Phenobarbital	MedlinePlus	Cat# a682007
Isofluorane	Henry Schein	Cat# 50562-1
Fluoromount-G	Southern Biotech	Cat# 0100-01
TTX	Alomone Labs	Cat# T-550
EZ-Link Biocytin	Thermo Fisher Scientific	Cat#28022
Glutamax	Thermo Fisher Scientific	Cat# 25030081
Critical Commercial Assays		
Papain dissociation system	Worthington Biochemical Corporation	LK003150
Illumina TotalPrep −96 RNA Amplification Kit	Ambion	IL1791
Illumina HumanHT-12_v4_BeadChip	Illumina	BD-103-0604
Aurum Total RNA Mini Kit	Bio-Rad	7326820
iScript Reverse Transcription Supermix	Bio-Rad	1708840
iTaq Universal SYBR Green Supermix	Bio-Rad	1725120
CFX connect Real-Time PCR Detection System	Bio-Rad	1855200
Deposited Data		
Microarray Data from Human Surgical Samples	This paper	NCBI GEO under project number GEO: GSE62019
Experimental Models: Organisms/Strains		
Mouse: *Emx-Cre; Clock*$^{flox/flox}$	This paper	N/A
Mouse: *PV-Cre; Clock*$^{flox/flox}$	This paper	N/A
Mouse: *Emx1-Cre*$^{+/-}$	Jackson Laboratory; Gorski et al., 2002	RRID: IMSR_JAX:005628
Mouse: *PV-Cre*$^{+/-}$	Jackson Laboratory; Hippenmeyer et al., 2005	RRID: IMSR_JAX:017320
Mouse: B6.129S4-Clock^{tm1Rep}/J	Jackson Laboratory; Debruyne et al., 2006	RRID: IMSR_JAX:010490
Oligonucleotides		
DBP forward primer: GAGCCTTCTGCAGGGAAACAG	This paper	N/A
DBP reverse primer: GAGTTGCCTTGCGCTCCTTTT	This paper	N/A
HLF forward primer: ACGATGGAGAAAATGTCCCG	This paper	N/A
HLF reverse primer: TTTCTTTACTAAATGCGTCTTCAGG	This paper	N/A
TEF forward primer: CCTTCCCTCTGGTCCTGAAGA	This paper	N/A
TEF reverse primer: CCTTCCCCTTTTCCTTATCGAG	This paper	N/A

REAGENT or RESOURCE	SOURCE	IDENTIFIER
GAPDH forward primer: TTGATGGCAACAATCTCCAC	This paper	N/A
GAPDH reverse primer: CGTCCCGTAGACAAAATGGT	This paper	N/A
Table S3 Primers used to create Clock shRNA plasmids	This paper	N/A
Software and Algorithms		
Ingenuity Pathways Analysis (IPA) software	QIAGEN	Cat# 830003
Partek Genomics Suite (version 6.5)	Partek	http://www.partek.com
Step-up False Discovery Rate multiple test adjustment	Benjamini and Hochberg, 1995	N/A
Co-localization Threshold	ImageJ	N/A